JGR Earth Surface

RESEARCH ARTICLE
10.1029/2021JF006450

The Hydrochemical Signature of Incongruent Weathering in Iceland

Trevor L. Cole[1], Mark A. Torres[1], and Preston C. Kemeny[2]

[1]Department of Earth, Environmental, and Planetary Sciences, Rice University, Houston, TX, USA, [2]Division of Geological and Planetary Sciences, California Institute of Technology, Pasadena, CA, USA

Key Points:

- New inverse model can explain the budgets of major and trace elements and their isotope ratios in Icelandic Rivers
- River compositions suggest preferential Na release relative to bulk Icelandic basalts
- Silicate weathering dominates the riverine alkalinity budget in Iceland

Supporting Information:

Supporting Information may be found in the online version of this article.

Correspondence to:

M. A. Torres,
mt61@rice.edu

Citation:

Cole, T. L., Torres, M. A., & Kemeny, P. C. (2022). The hydrochemical signature of incongruent weathering in Iceland. *Journal of Geophysical Research: Earth Surface*, *127*, e2021JF006450. https://doi.org/10.1029/2021JF006450

Received 27 SEP 2021
Accepted 2 JUN 2022

Author Contributions:

Conceptualization: Trevor L. Cole, Mark A. Torres
Data curation: Trevor L. Cole
Formal analysis: Trevor L. Cole
Funding acquisition: Mark A. Torres
Methodology: Trevor L. Cole
Project Administration: Mark A. Torres
Resources: Mark A. Torres
Software: Trevor L. Cole, Preston C. Kemeny
Supervision: Mark A. Torres
Visualization: Mark A. Torres
Writing – original draft: Trevor L. Cole, Mark A. Torres
Writing – review & editing: Mark A. Torres, Preston C. Kemeny

Abstract Basaltic watersheds such as those found in Iceland are thought to be important sites of CO_2 sequestration via silicate weathering. However, determining the magnitude of CO_2 uptake depends on accurately interpreting river chemistry. Here, we compile geochemical data from Iceland and use them to constrain weathering processes. Specifically, we use a newly developed inverse model to quantify solute supply from rain and hydrothermal fluids as well as allow for variable silicate end-member compositions, solutes to be removed via secondary phase formation, and some Ca to be sourced from carbonate dissolution. While some of these processes have been considered previously, they have not been considered together allowing us to newly determine their relative contributions. We find that weathering in Iceland is incongruent in two ways. First, solute release from primary silicates is characterized by a higher proportion of Na than would be expected from bulk basalts, which may reflect preferential weathering or some contribution from rhyolites. This Na enrichment is further enhanced by preferential Mg and K uptake by secondary phases. No samples in our data set ($n = 537$) require carbonate dissolution even if isotopic data (δ^{26}Mg, δ^{30}Si, δ^{44}Ca, and/or $^{87}Sr/^{86}Sr$) are included. While some carbonate weathering is allowable, silicate weathering likely dominates. The complexity we observe in Iceland underscores the need for inverse models to account for a wide range of processes and end-members. Given that riverine fluxes from Iceland are more Na-rich than expected for congruent basalt weathering, the characteristic timescale of CO_2 drawdown is likely affected.

Plain Language Summary The chemical composition of rivers can be used to determine how processes occurring at Earth's surface affect climate. Here, we use measurements from rivers in Iceland because it is an ideal test case since geologic factors are expected to simplify the interpretation of river chemistry. Using a new approach, we identify a range of processes that affect Icelandic rivers and quantify their relative importance. While it was assumed that the results would be "simple," we instead find complicated behavior, which is important to understand when applying similar approaches to much larger rivers. We also find that the way rivers in Iceland affect the climate is slightly different than originally expected. Nevertheless, these rivers still act to remove carbon dioxide from the atmosphere and thus cool the climate.

1. Introduction

Silicate mineral dissolution promotes the removal of CO_2 from the ocean–atmosphere system by providing the cations and alkalinity necessary for carbonate mineral burial, which is the primary geologic sink for CO_2 released from solid Earth degassing and sedimentary recycling (Berner et al., 1983). Though the dissolution of carbonate minerals also supplies alkalinity to the ocean, carbonate weathering alone cannot drive net carbonate burial and thus influences CO_2 consumption over shorter timescales compared to silicate weathering (Broecker & Sanyal, 1998). Therefore, quantifying the fractional contribution of cations derived from silicate versus carbonate mineral dissolution during chemical weathering is critical to understanding the geologic C cycle.

The main factors that modulate silicate weathering fluxes are thought to include climate, lithology, and uplift/erosion rates. These mechanisms have been explored through numerous field studies of riverine solute fluxes (e.g., Bluth & Kump, 1994; Eiriksdottir et al., 2013; Ibarra et al., 2016; West et al., 2005) as well as laboratory experiments (e.g., Chen & Brantley, 1997; Gislason & Oelkers, 2003; Gudbrandsson et al., 2008; Schaef & McGrail, 2009; Taylor et al., 2000; Wolff-Boenisch et al., 2004). Overwhelmingly, these investigations highlight lithology as a major control on weathering fluxes and suggest that mafic lithologies ("basalts") chemically weather 2–10 times faster than felsic lithologies ("granites"; Bluth & Kump, 1994; Ibarra et al., 2016). So, despite the fact that basalts occupy only ~5% of exoreic land surface area, solute fluxes from these areas may contribute

disproportionately to C sequestration by accounting for 30%–35% of the global contemporary silicate weathering flux (Dessert et al., 2003). The weathering of mafic lithologies like basalt also factors in to current interpretations of the drivers of geologic climate change. For example, models disagree on whether Cenozoic cooling reflects an increase (Park et al., 2020) or decrease (G. Li & Elderfield, 2013) in global basalt weathering fluxes, highlighting the need for a more mechanistic understanding of mafic weathering processes.

The interpretation that basalts contribute disproportionately to modern silicate weathering fluxes is based on measurements of the dissolved chemistry of rivers and therefore is predicated on our ability to accurately partition riverine solutes between different solute sources such as atmospheric deposition, silicate mineral dissolution, and carbonate mineral dissolution (Bickle et al., 2015; Gaillardet et al., 1999; Kemeny et al., 2020; Moon et al., 2014; Négrel et al., 1993; Torres et al., 2016). While common igneous rock types are nominally considered to contain purely silicate minerals, they often contain accessory carbonate minerals in trace amounts (White et al., 1999, 2005). Due to their high reactivity, carbonates can contribute appreciably to solute loads even when present at low abundances in bedrock (D. Li et al., 2014).

Existing global analyses of basaltic weathering fluxes based on river chemistry have mostly assumed that there is a negligible contribution from accessory carbonates (Dessert et al., 2003; Ibarra et al., 2016; G. Li et al., 2016). If this assumption about solute sources is in error, as implied by interpretations of either the stable isotopic compositions of dissolved calcium and strontium (Andrews & Jacobson, 2017; Jacobson et al., 2015) or major element concentrations (Georg et al., 2007) in some basalt-draining watersheds in Iceland, then our understanding of global basalt weathering may be incomplete. On the other hand, the chemical signals in river waters that are thought to be indicative of carbonate mineral dissolution (i.e., differences in elemental and stable isotopic ratios relative to primary silicates) can be generated by other geochemical processes such as the formation of secondary phases like clay minerals (Hindshaw et al., 2013). If it is the case that carbonate weathering meaningfully contributes to solute fluxes in basaltic watersheds, prior studies could potentially have over-emphasized the role of basaltic landscapes in stabilizing the geologic carbon cycle by sequestering atmospheric CO_2.

Evidence that secondary clay formation modulates the chemical composition of Icelandic rivers, and basalt-draining rivers in general, exists in the form of mineral mass balance calculations (Moulton et al., 2000), reaction path modeling (Stefánsson & Gíslason, 2001), the isotopic composition of dissolved Si and Li (Georg et al., 2007; Opfergelt et al., 2013; Pogge von Strandmann et al., 2006), and direct measurements of clay mineralogy and elemental composition (Crovisier et al., 1992; Ehlmann et al., 2012; Moulton et al., 2000; Thorpe et al., 2019; Wada et al., 1992). However, explanations of river chemistry that appeal to multiple solute sources (carbonate vs. silicate) or fractionation by secondary clay formation are not mutually exclusive. As such, effective hypothesis testing requires models that consider a range of processes together. Specifically, recent work has shown that the formation of secondary minerals biases inferences of carbonate versus silicate mineral weathering in river chemistry data such that models must explicitly account for both processes in order to yield accurate results (Bickle et al., 2015; Emberson et al., 2017, 2018).

In some past work on weathering in Iceland, it has been assumed that silicate weathering processes release solutes in similar ratios to bulk basalts (Gíslason et al., 1996; Jacobson et al., 2015; Kemeny et al., 2021; Stefánsson et al., 2001) or some mixture of bulk basalts and bulk rhyolites (Louvat et al., 2008). The assumption of congruent solute release (i.e., similar elemental ratios for rivers as in bulk rocks) may be reasonable for catchments where volcanic glass weathering dominates as experiments show the congruent release of major cations from basaltic glass (Gislason & Eugster, 1987). However, for more crystalline bedrock, the fact that not all minerals react at the same rate under like conditions may lead to effective solute release ratios that are substantially different from the bulk rock composition (Emberson et al., 2017; Gislason & Eugster, 1987; Ryu et al., 2011). Deviations in effective end-member compositions relative to the bulk rock depend on a myriad of factors (e.g., weathering duration; Ferrier & Kirchner, 2008) such that compositions near the bulk rock value may be reasonably accurate for some crystalline lithologies under some circumstances. Nevertheless, observations of differential rates of primary mineral depletion in basaltic soil profiles from Hawaii (Ryu et al., 2014) suggests that silicate end member compositions that do not exactly match bulk rocks must be considered alongside secondary clay formation when trying to interpret river chemistry in terms of the lithologic sources of solutes.

The details affecting river water chemistry are ultimately important as they can influence the magnitude of CO_2 drawdown by weathering and the characteristic timescales over which this drawdown applies. In much previous

work, the effects of basaltic watersheds on the C cycle have been determined using bicarbonate fluxes (Dessert et al., 2003; Ibarra et al., 2016; G. Li et al., 2016), which implicitly assumes that all dissolved cations contribute to CO_2 drawdown equally over the same timescales. This is not the case, however, as the major processes that remove seawater alkalinity associated with Na^+, K^+, and Mg^{2+} ions (i.e., "reverse weathering"; Mackenzie & Garrels, 1966) are different from those that remove seawater alkalinity associated with Ca^{2+} ions. By altering the proportion of silicate weathering derived alkalinity associated with Ca relative to what is implied by the bulk bedrock composition, varying rates of primary mineral dissolution and/or extent of solute uptake into secondary minerals can affect the links between weathering and the long-term C cycle. Additionally, significant cation retention in secondary minerals effectively decreases the amount of alkalinity generated by weathering and could be one of the factors that explains observed differences in solute generation between basaltic watersheds (Dessert et al., 2003; Ibarra et al., 2016; G. Li et al., 2016).

To make progress on understanding silicate weathering in volcanic terrains, we combine published measurements of bedrock and water chemistry from Iceland and analyze them using an inverse model that allows for multiple solute sources (rainwater, hydrothermal fluids, silicates, and carbonates) and solute fractionation mechanisms (secondary phase formation and variable silicate end-member compositions). Our definition of solute fractionation aligns with the more generic term incongruent weathering, which, in the literature, has been used to refer to instances where solutes released by weathering are taken up into secondary phases (Misra & Froelich, 2012) as well as when solutes are released into solution in a different ratio relative to the bulk solid, but no new phases are formed (e.g., due to different rates of primary mineral dissolution or grain-scale effects; Bickle et al., 2015; Rickli et al., 2013; Ruiz-Agudo et al., 2012). For clarity, we separate these two concepts and refer to them as secondary phase incongruence and primary mineral incongruence, respectively. The structure of our modeling approach allows us to discern how primary and secondary incongruence influence the partitioning of solute loads between carbonate and silicate sources in a system where the bedrock chemistry is relatively uniform and well-known. Understanding solute source apportionment in such systems is a prerequisite for interpreting more lithologically-complex river systems in terms of their effects on the global C cycle.

2. Methods

2.1. Hydrochemistry

2.1.1. Data Compilation

Previously published solute concentrations, water quality parameters (pH, temperature, and water type classification) as well as geospatial data for water samples collected in Iceland were identified through Web of Knowledge and transcribed into an Excel® database through a combination of electronic transfer and manual tabulation. For this work, we emphasized data from rivers, but our compilation includes a range of other water sample types. Specifically, we distinguish 10 water types: rain waters, cold springs, glacial rivers, groundwater wells, hydrothermal fluids, lake waters, multi-sourced rivers, non-glacial rivers, soil pore waters, and unclassified rivers. In addition to these classifications, we also group all of the river water data types together (labeled river waters) as well as group the groundwater well, cold spring, and soil pore water samples together (labeled sub-surface waters; Figure 1). We focused on collecting data for major solute concentrations (i.e., Cl, SO_4, Na, K, Ca, Mg, Si), but if additional trace elements and isotopic ratio data were available, we included them in our database. In our database, Ca isotopic ratios are reported as both $^{44}Ca/^{42}Ca$ and $^{44}Ca/^{40}Ca$ values normalized to either the SRM915a or OSIL seawater standard, respectively. For the analyses reported here, we converted all Ca isotopic data to $^{44}Ca/^{40}Ca$ values normalized to the OSIL seawater standard.

When geographical coordinates of sampling locations were provided, they were converted to datum ISN1993 and recorded in decimal degrees. If a sample location was not provided but a map was, an attempt was made to approximate the sample location using Google Earth® (Gíslason et al., 1996; Mutonga et al., 2010; Oskarsson et al., 2013; Scott et al., 2014; Stefánsson & Gíslason, 2001). Coordinates for the sampling locations associated with the data reported in Gislason and Arnórsson (1993) and Stefánsson et al. (2001) are not available due to a lack of sample location map or provided locality data. A map showing all of the sample locations is provided in Figure 1.

An effort was made to classify river water types (i.e., glacial or non-glacial river) if a description was not provided but a sample location was by using visual observations of river turbidity in Google Earth imagery.

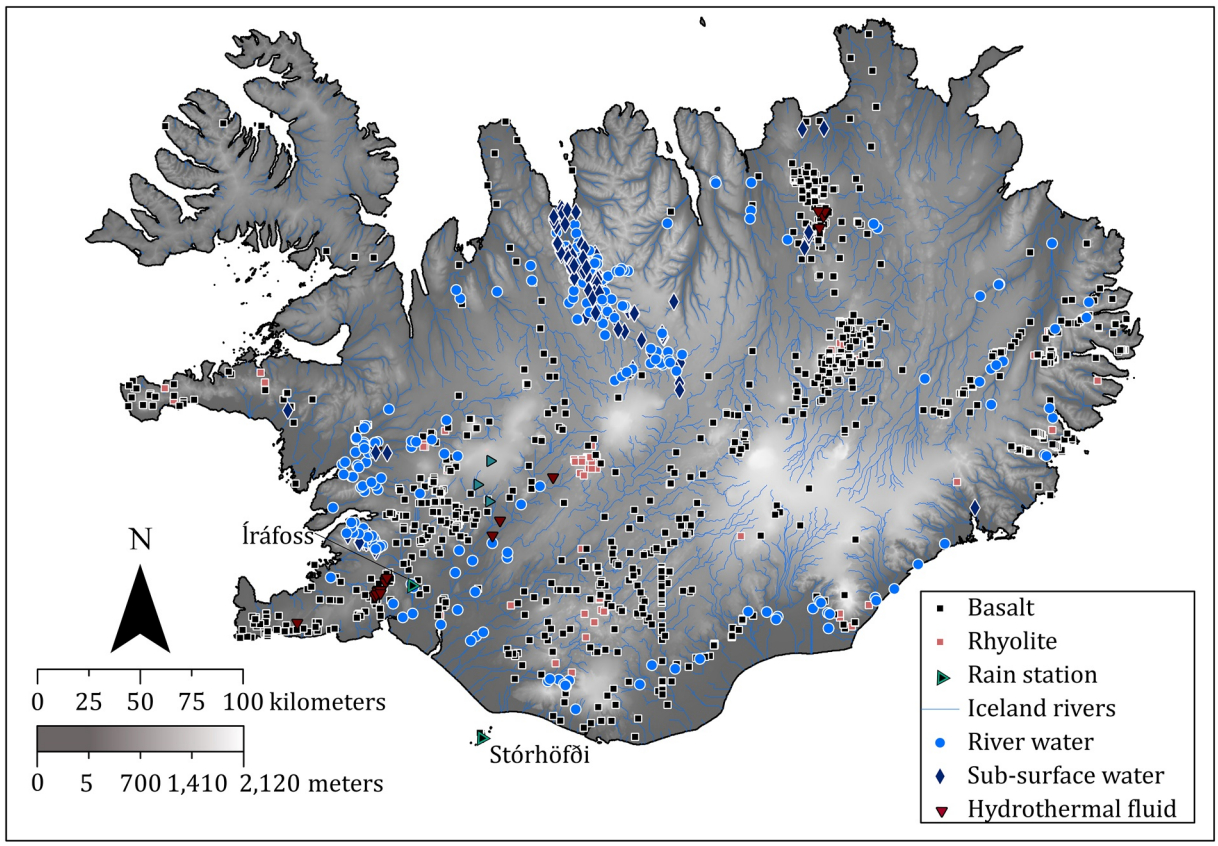

Figure 1. Shaded relief map showing the sampling locations for the river waters (light blue circles), sub-surface waters (dark blue diamonds), rain station (light blue triangle with black center), rain waters (light blue triangles), hydrothermal fluids (red triangles), basalts (black squares), and rhyolites (light red squares) used in this study.

We note that the data reported by Gíslason et al. (1996) and Moulton et al. (2000) represent average concentrations from multiple measurements and that the individual data points were not provided by the authors. In some cases, time-series of multiple observations from an individual site were reported (e.g., Eiriksdottir et al., 2013) and, in our analysis, each sample is considered independently. Other sources report single observations from a given locality (e.g., Jacobson et al., 2015). In total, 22 publications were compiled amounting to 1,432 observations (Andrews & Jacobson, 2017; Arnórsson et al., 2002; Eiriksdottir et al., 2013; Gannoun et al., 2006; Georg et al., 2007; Gislason & Arnórsson, 1993; Gíslason et al., 1996, 2006; Hindshaw et al., 2013; Jacobson et al., 2015; Louvat et al., 2008; Moulton et al., 2000; Mutonga et al., 2010; Olsson et al., 2014; Oskarsson et al., 2013; Pogge von Strandmann et al., 2006; Pogge von Strandmann, Olsson, et al., 2019; Scott et al., 2014; Stefánsson & Gíslason, 2001; Stefánsson et al., 2001; Vigier et al., 2006, 2009).

Data for the chemical composition of Icelandic rainwater was taken from the co-operative program for monitoring and evaluation of the long-range transmission of air pollutants in Europe (EMEP) along with two rainwater samples and one glacial meltwater sample from Gannoun et al. (2006) and Pogge von Strandmann et al. (2006) collected near Langjökull (Figure 1). The EMEP provides time-series data for two sites in Iceland: Íráfoss and Stórhöfði (Figure 1). Here, we primarily focus on 96 monthly and annually averaged rainwater samples from the Íráfoss site, which has measurements for major cations and anions for the time period 2006–2012 as well as 2015. Rainwater data from the Stórhöfði site match the elemental ratios expected for seawater and show much higher solute concentrations than at Íráfoss. The higher concentrations observed at the Stórhöfði site may relate to the fact that this site is much closer to the ocean compared to Íráfoss (Figure 1). The monthly data from the Íráfoss site are more variable in terms of solute concentrations and ratios compared to the Stórhöfði site, but still encompass seawater-like elemental ratios.

While the rain water samples from Stórhöfði, Íráfoss, and Langjökull are all broadly similar in terms of elemental ratios, they are all also located in the southwestern part of Iceland and thus we lack strong constraints on rainwater chemistry in the other regions of Iceland where some of the river water samples are located (Figure 1). In some past studies of river chemistry in northeastern Iceland (e.g., Eiriksdottir et al., 2013), rainwater has been assumed to have an identical composition to seawater. Our approach here to use data from the Íráfoss site to characterize variability in rainwater chemistry across Iceland is thus consistent with past assumptions, but improves upon them by allowing for realistic, data-informed variations.

2.1.2. Data Quality Control

For the river and subsurface water analyses, we removed samples where concentrations for either Cl, Na, K, Ca, Mg, or Si were missing or reported as zero in the primary publication. We also removed river and subsurface water where the total charge of major anions (Cl and SO_4) exceeded the total charge of major cations (Na, K, Ca, and Mg). For thermodynamic calculations (see Supporting Information S1), we applied a more stringent, charge-balance based threshold to the river and subsurface waters. For the remaining water types, namely the rain and hydrothermal waters, we did not apply any quality control procedures.

2.1.3. Data Normalization

For many of our analyses, we use ratios of solute concentrations in order to focus on variations in solute sources instead of other factors, such as evaporation, dilution, and variable extent of reaction, that can independently influence measured concentrations. Multiple options are available to convert a solute concentration (X; μM) to a ratio. For example, individual cations (X/Na; Négrel et al., 1993), sums of a subset of cations (X/Na + Ca), or sums of cations and anions (X/Na + SO_4; Blattmann et al., 2019) could all be used as normalization variables. The choice of normalization variable is important as mixing analyses cannot model end-members that contribute solely to an element that is not in the normalization variable. For example, if Na is used as the normalization variable, it must be assumed that carbonate dissolution also contributes to the Na budget.

For visualization, we normalize the individual solute concentrations by the sum of Na, K, Ca, and Mg concentrations (Σ^+; μM) because most end-member solute sources contribute to the budget of at least one major cation. For inverse analysis of solute sources (see below), we use the sum of Σ^+ and sulfate concentrations ($\Sigma^\pm$; μM) as a normalization variable in order to model sulfide mineral oxidation as an independent process that releases sulfate, but not major cations. This approach of normalizing by sums of solute concentrations has some important implications for data analysis. For example, the X/Σ^+ values for Na, K, Ca, and Mg have the property of each being confined to the interval 0–1 and, for a single sample, the four ratios must all sum to a value of 1 (unit sum constraint). For elements not included in the denominator term, which, for Σ^+, includes Si, Cl, and SO_4, X/Σ^+ can exceed 1. However, SO_4/Σ^+ or Cl/Σ^+ values much greater than 1 would imply a charge imbalance unless other cations (e.g., Fe^{2+} and/or H^+) were present at sufficient levels in solution. For elements that are included in the denominator term, uncertainties in X/Σ^+ values are correlated.

2.2. Solid Phase Compositions: Compilation and Analysis

Icelandic bedrock elemental abundances and sampling locations were primarily taken from the Geochemistry of Rocks of the Oceans and Continents (GEOROC) database. Additional solid-phase geochemical data, including measurements of sieved sediment samples and soils as well as mineral abundances, were taken from the literature (Moulton et al., 2000; Thorpe et al., 2019). All bedrock samples were classified into different rock types (basalt, dacite, rhyolite, etc.) according to a scatterplot of the sum of sodium and potassium concentrations and silica concentrations.

As a quality control measure for the GEOROC data set, samples where any of the concentrations of Al, Ca, K, Mg, Na, or Si deviated more than three scaled median absolute deviations from the median concentration for that element were excluded from our data analysis, which was accomplished using the MATLAB function `isoutlier()`. In total, 6,887 bedrock samples were retained out of initial data set of 7,849 and used in subsequent analyses (88% retention).

To constrain the composition of secondary precipitates, we used soil and sediment samples in our database where the authors sieved to <2 μm prior to analysis (Moulton et al., 2000; Thorpe et al., 2019). While analyses presented in these original publications confirm that such samples are enriched in phyllosilicate mineral phases,

it is unlikely that they are perfectly pure and may instead contain some finely ground primary minerals. Accordingly, we use these data as a loose guide on the composition of secondary phyllosilicates. For the data from Moulton et al. (2000), we also consider their reported measurements with and without a correction for contamination from atmospheric deposition based on reported Cl concentrations and seawater element to chloride ratios (see discussion in Stefánsson and Gíslason [2001]).

2.3. Solute Mass Balance Modeling Using MEANDIR

2.3.1. Overview

Models for interpreting the chemical composition of rivers in terms of weathering processes range in complexity. For example, the mineral mass balance approach of Garrels and Mackenzie (1967) allows for multiple mineral phases to both dissolve and precipitate with the important constraint that the composition of each phase must be known (Moulton et al., 2000). In contrast, the inversion approach of Négrel et al. (1993) groups all silicate minerals together and does not allow for any secondary mineral formation, but is less demanding in terms of the prior knowledge required to employ the model. Here, we utilize an intermediate complexity approach that accounts for secondary mineral formation without the strict data requirements of a full mineral mass balance. Our method is similar to the approach of Bickle et al. (2015), but differs in that we consider secondary silicate phases rather than secondary carbonate phases and are more flexible in our definition of the silicate end-member. A full description of our inversion model is given in Kemeny and Torres (2021) and the associated software, titled "Mixing Elements and Dissolved Isotopes in Rivers (MEANDIR)," is available as MATLAB code. Below, we describe relevant aspects of the model and its application to the Icelandic data set.

Based on expectations from prior research, we assume that rivers in Iceland source solutes from rain water, hydrothermal fluids, silicate mineral dissolution, low-Mg carbonate mineral dissolution, and sulfide mineral oxidation. Additionally, solutes may be removed by the formation of secondary phases. For the silicate end-member, we utilize four separate components (i.e., one for each major cation) in order to avoid the assumption that this end-member must look like bulk rocks. This results in nine unique end-members. Using our solution scheme (see below), it is possible to solve for the fractional contributions from this set of 9 end-members using Cl, SO_4, Na, K, Ca, Mg, and Si concentration measurements alone, which are available for 537 quality-controlled river water samples. To evaluate the results we obtain using only major elements, we perform additional simulations using the subset of river samples with additional trace element and isotopic data. Specifically, we use a subset of 24 samples with measurements of Sr concentrations, $^{87}Sr/^{86}Sr$, and $\delta^{44}Ca$ as well as a subset of 7 river water samples where measurements of $\delta^{26}Mg$ and $\delta^{30}Si$ are also available in addition to Ca and Sr isotopic ratios. In some instances, linking the isotopic measurements to the major element data required matching sample identifiers between published studies.

2.3.2. MEANDIR Inversion Equations

For Na, K, Ca, Mg, Sr, Si, SO_4, and Cl, we utilize the mass balance equation:

$$\left(\frac{X_i}{\Sigma^{\pm}}\right)_{riv} = \sum_{j=1}^{n} f_j \cdot \left(\frac{X_i}{\Sigma^{\pm}}\right)_j \tag{1}$$

where $X_i/\Sigma^{\pm}$ is the ratio of element i to the sum of major cations (Na, K, Ca, and Mg) and sulfate measured in a river sample (subscript *riv*) or assumed for an end-member (subscript j) and f_j is the fractional contribution of end-member j to the net budget of the normalization variable. To force primary minerals to dissolve and secondary minerals to precipitate, we constrain the model to only find solutions where the f_j values are either positive (dissolution) or negative (precipitation) depending on the end-member.

To add strontium isotopic ratios to our mass balance framework, we utilize the equation:

$$\left(\frac{^{87}Sr}{^{86}Sr}\right)_{riv} \cdot \left(\frac{Sr}{\Sigma^{\pm}}\right)_{riv} = \sum_{j=1}^{n} f_j \cdot \left(\frac{^{87}Sr}{^{86}Sr}\right)_j \cdot \left(\frac{Sr}{\Sigma^{\pm}}\right)_j \tag{2}$$

While Equation 2 represents a relatively standard approach for incorporating isotopic data into river inversion models (Négrel et al., 1993), we note that our application here is complicated by the fact that we allow for solutes

to be removed from solution by secondary mineral formation (i.e., f_j for the clay end-member is constrained to be ≤0). Consequently, it is mathematically possible for the extent of clay formation to shift dissolved $^{87}Sr/^{86}Sr$ values if, for example, the isotopic composition of Sr supplied by weathering, atmospheric deposition, and/or hydrothermal inputs does not match the isotopic composition of Sr incorporated into clays. In order to avoid such a mathematical fractionation of $^{87}Sr/^{86}Sr$ by clay formation, we set the $^{87}Sr/^{86}Sr$ of clays to be equal to the weighted average isotopic composition of all of the solute sources in each model simulation.

In contrast to $^{87}Sr/^{86}Sr$, we *do* expect clay formation to naturally fractionate Mg, Si, and Ca isotopic ratios. Accordingly, we incorporate these isotopic systems using a different approach. To model the isotopic fractionation associated with clay formation, we adapt the model of Bouchez et al. (2013), which relates the isotopic composition of river water to the extent of element uptake using the expression:

$$\delta^X_{riv} - \delta^X_{source} = F^X_{clay} \cdot \Delta^X \quad (3)$$

where δ^X_{riv} is the isotopic ratio of element X measured in a river sample, δ^X_{source} is the contribution-weighted average isotopic ratio of element X supplied from all solute sources, F^X_{clay} is the fraction of all of element X supplied to the weathering system that is taken up into secondary clays, and Δ^X is the fractionation factor for element X incorporation into secondary clays. We adapt the Bouchez et al. (2013) model as mixing in river systems causes departures from Rayleigh-type behavior that can be approximated by this type of linear model (Druhan & Maher, 2017). For each simulation, F^X_{clay} is constrained by the calculated f_j values and selected end-member compositions. To determine δ^X_{source}, we weight end-member isotopic ratios for rainwater, silicates, carbonates, and hydrothermal fluids (Table 1) by the inversion model results for their fractional contributions. We specify an allowable range for Δ^X for each isotopic system based on published experimental and field data (Section 2.3.3; Table 1).

In essence, MEANDIR assumes a well-mixed system where all solutes supplied by weathering or mixing are able to participate in secondary reactions. This assumption is common to most treatments of isotopic data from river systems (Bouchez et al., 2013). Nevertheless, it could be violated in systems with a very heterogeneous and segregated critical zone in terms of fluid and solid compositions. Given overall low weathering intensities in Iceland (Dellinger et al., 2015) and the prevalence of near-surface bedrock, we think that the well-mixed assumption is not violated to a degree that would completely invalidate the model results.

2.3.3. End-Member Definitions

For rainwater Na-, K-, Ca-, Mg-, Cl-, and SO_4 to $\Sigma^{\pm}$ ratios, we use the full range of major element compositions displayed by monthly values at the Íráfoss site in the EMEP. Further, we assume that rainwater contains negligible Si (Wilkinson et al., 1997) and that seawater Sr to Ca ratios can be used to estimate the rainwater Sr to $\Sigma^{\pm}$ ratio based on our assumed range of $Ca/\Sigma^{\pm}$. For rainwater Ca, Mg, and Sr isotopic ratios, we use seawater-like values assuming that seawater-derived aerosols are the primary source of these elements in rainwater. We note that the atmospheric deposition flux of anthropogenic S has likely decreased over time in Iceland (Gislason & Torssander, 2006) and some of our river water data were collected prior to EMEP observations. Any potential excess anthropogenic S not accounted for by the rainwater end-member would ultimately get incorporated into the sulfide oxidation end-member (Kemeny & Torres, 2021). As we do not directly interpret our apportionment of the sulfide budget, our analysis here is unaffected. Nevertheless, it may be most accurate to interpret the sulfide oxidation end-member as a combination of true sulfide mineral oxidation and anthropogenic S emissions.

For the hydrothermal end-member, we take the range defined by the measurements of samples in our database with temperatures over 100°C as these are assumed to better represent "pure" hydrothermal fluids. We assume that hydrothermal fluids contain negligible Mg ($Mg/\Sigma^{\pm} = 0$) and allow $SO_4/\Sigma^{\pm}$ to range from 0 to 0.1. For Ca, Mg, Sr, and Si isotopic ratios, we use data from Elderfield and Greaves (1981), Pogge von Strandmann et al. (2008), Hindshaw et al. (2013), and Opfergelt et al. (2013).

For the carbonate end-member, we assume that it contains negligible amounts of Na and K, but allow Mg/Σ^{+} to range between 0 (stoichiometric carbonate) and 0.05, which is in line with measurements of Icelandic carbonates (Harstad & Stipp, 2007). We parameterize that Sr/Σ^{+}, $\delta^{44}Ca$, and $^{87}Sr/^{86}Sr$ of the carbonate end-member using measurements from Jacobson et al. (2015) and Andrews and Jacobson (2017). We use data

Table 1
End-Member Compositions Used in the Solute Mass Balance Model

		Pyrite	Precipitation	Hot spring	Clay	Carbonate	Na-silicate	K-silicate	NaK-silicate	Mg-silicate	Ca-silicate
$Na/\Sigma^{\pm}$	Min		0.6	0.8	0		1		0		
$Na/\Sigma^{\pm}$	Max		0.9	0.95	0.25		1		1		
$K/\Sigma^{\pm}$	Min		0.02	0.05	0.05			1	0		
$K/\Sigma^{\pm}$	Max		0.2	0.12	0.3			1	1		
$Ca/\Sigma^{\pm}$	Min		0.02	0	0.2	0.95					1
$Ca/\Sigma^{\pm}$	Max		0.1	0.01	0.45	1					1
$Mg/\Sigma^{\pm}$	Min		0.05		0.75	0				1	
$Mg/\Sigma^{\pm}$	Max		0.1		1	0.05				1	
$Cl/\Sigma^{\pm}$	Min		0.6	0.4							
$Cl/\Sigma^{\pm}$	Max		1.2	0.9							
$SO_4/\Sigma^{\pm}$	Min	1	0.014	0							
$SO_4/\Sigma^{\pm}$	Max	1	0.1	0.1							
$Sr/\Sigma^{\pm}$	Min		1.00E-04	1.00E-06	1.00E-05	1.00E-06	1.00E-06	1.00E-06	1.00E-06	1.00E-06	1.00E-06
$Sr/\Sigma^{\pm}$	Max		3.00E-04	1.00E-04	3.00E-03	1.00E-04	1.00E-03	1.00E-03	1.00E-03	1.00E-04	1.00E-03
$^{87}Sr/^{86}Sr$	Min		0.7091	0.703	Source	0.7031	0.703	0.703	0.703	0.703	0.703
$^{87}Sr/^{86}Sr$	Max		0.7093	0.704	Source	0.7034	0.704	0.704	0.704	0.704	0.704
$Si/\Sigma^{\pm}$	Min			0.2	2		1	1	1	1	1
$Si/\Sigma^{\pm}$	Max			3	10		3	3	3	2	2
$\Delta^{44}Ca$	Min				−1.5						
$\Delta^{44}Ca$	Max				+0.5						
$\Delta^{26}Mg$	Min				−1.5						
$\Delta^{26}Mg$	Max				+1						
$\Delta^{30}Si$	Min				−2						
$\Delta^{30}Si$	Max				+0.5						
$\delta^{44}Ca$	Min		−0.5	−1.1		−0.9					−2
$\delta^{44}Ca$	Max		0.5	−0.8		−0.5					−1
$\delta^{26}Mg$	Min		−0.83			−4				−0.5	
$\delta^{26}Mg$	Max		−0.81			−0.2				−0.2	
$\delta^{30}Si$	Min			−0.5			−0.5	−0.5	−0.5	−0.5	−0.5
$\delta^{30}Si$	Max			1			−0.2	−0.2	−0.2	−0.2	−0.2

from Pogge von Strandmann, Olsson, et al. (2019) to parameterize the Mg isotopic composition of hydrothermal carbonate. Following past studies of Icelandic rivers showing under-saturation with respect to carbonate phases (e.g., Hindshaw et al., 2013), we do not allow for secondary carbonate formation in our model. In cases when the compositions of primary and secondary carbonates are similar, MEANDIR does not distinguish between simulations with more secondary carbonate formation and simulations with less primary carbonate dissolution (Kemeny & Torres, 2021).

For the solute sink, we make slight adjustments to the ranges of elemental ratios displayed by the fine-grained sediment data presented in Moulton et al. (2000) and Thorpe et al. (2019). Specifically, we allow for lower $Ca/\Sigma^{\pm}$ values (0.2–0.45 instead of the 0.3–0.5 range displayed by the data) and higher $Mg/\Sigma^{\pm}$ values (0.75–1 instead of the 0.3–0.4 range displayed by the data). These differences are justified because the grain-size separates from Moulton et al. (2000) and Thorpe et al. (2019) may contain some primary silicate minerals in addition to secondary phases. Further, we allow $Si/\Sigma^{\pm}$ to range between 2 and 10, which is wider than the observed range of 2.5–6. The higher $Si/\Sigma^{\pm}$ values are included to account for the formation of amorphous Si and/or aluminosilicates (e.g.,

allophane and immogolite) that may only sequester low concentrations of cations via adsorption. For $Sr/\Sigma^{\pm}$, we assume a wide range from roughly 1×10^{-5} to 3×10^{-3} given the lack of direct measurements (Table 1). While we label and parameterize this solute sink as a clay mineral, we note that our analysis approach will assign any biotic solute uptake to this end-member. Based on the results of Moulton et al. (2000), it is likely that clay formation dominates solute uptake compared to biota in Iceland.

In lieu of specifying the Ca, Mg, and Si isotopic ratios of secondary phases, we instead specify a range of allowable fractionation factors for each isotope system. Moreover, we deliberately select a slightly wider range of fractionation factors relative to existing observations to account for uncertainties and limit the influence of the a priori distribution on the modeling results. By examining the posterior distributions of fractionation factors, we are able to determine whether or not "extreme" values outside our existing understanding are required to explain the observations. For each isotopic system, we also allow for fractionation factors of 0‰, which, in effect, requires all observed variations in isotopic ratios to be driving by the mixing of isotopically distinct sources. So, even though we include a solute sink in our model, we are able to directly test its importance to isotopic budgets by including scenarios where it has no impact.

For Si isotopic ratios, we use a range of $\Delta^{30}Si$ from −2 to +1‰. Though most clays preferentially take up ^{28}Si (i.e., negative $\Delta^{30}Si$; Baronas et al., 2020; Cornelis et al., 2014; Ziegler, Chadwick, White, & Brzezinski, 2005), we allow for slightly positive Si fractionation factors given experimental data for amorphous Si (Roerdink et al., 2015; Zheng et al., 2019) and the possibility that it may serve as a precursor for clays and/or affect river chemistry by adsorbing cations. Likewise, we use a range from −1.5 to +1‰ for $\Delta^{26}Mg$ based on experimental data showing that the sign of the Mg fractionation factor can be variable for clays depending on the Mg-O bond length (Hindshaw et al., 2020). For the Ca isotopic system, there is limited experimental data for clay minerals. Nevertheless, adsorption onto clay surfaces imparts a range of fractionation factors from −2.7 to +0.06 (Brazier et al., 2019; Ockert et al., 2013), though the largest fractionation factors are observed at seawater ionic strength. Accordingly, we use a prior distribution of $\Delta^{44}Ca$ from −1.5 to +0.5 to account for the present uncertainty.

For the composition of the silicate end-member, we use a novel approach that allows for primary mineral incongruent weathering. Specifically, we break the silicate end-member into four separate components: Na-silicate ($Na/\Sigma^{\pm} = 1$), K-silicate ($K/\Sigma^{\pm} = 1$), Ca-silicate ($Ca/\Sigma^{\pm} = 1$), and Mg-silicate ($Mg/\Sigma^{\pm} = 1$). In effect, this allows the silicate end-member to take on any composition and uses the data to constrain the best-fitting values. This contrasts with the approach used in prior inversion models where a single silicate end-member is used and assumed to have a composition similar to bulk Icelandic basalts. In effect, this restricts the expression of primary mineral incongruence to the uncertainty assigned to the silicate end-member composition. We assign all silicate end-members the same prior distributions for $Sr/\Sigma^{\pm}$, $^{87}Sr/^{86}Sr$ (Condomines et al., 1983; Hemond et al., 1988; O'nions & Grönvold, 1973; Sun & Jahn, 1975), and $\delta^{30}Si$ (Georg et al., 2007). However, since each of the four silicate end-members are independent, they need not have identical values for these ratios in a given simulation. In effect, this captures the slight differences in isotopic ratios between igneous materials that results from magmatic differentiation (e.g., Savage et al., 2011). For Ca and Mg isotopic ratios, we use constraints from Jacobson et al. (2015), Andrews and Jacobson (2017), and Pogge von Strandmann et al. (2008).

2.3.4. MEANDIR Solution Scheme

We utilize a Monte-Carlo approach to sample the full range of possible end-member compositions. Specifically, we generated random sets of end-member ratios from their defined ranges assuming uniform distributions (Section 2.3.3; Table 1) excluding combinations that violated the unit sum constraint. All inversion model formulations are solved using a cost-function that minimizes the proportional error of each solute using the MATLAB function `fmincon()`. For isotopic systems expressed in delta notation, this approach requires converting the delta values to absolute isotopic ratios. When using only the major elements as model constraints, an additional Monte-Carlo draw of the relative contributions from the Na- and K-silicate end-members is necessary prior to performing the constrained optimization as, otherwise, the system of equations is under-constrained (see NaK-silicate end-member in Table 1). In effect, this makes the parameter search less efficient (i.e., more model iterations are required), but full range of possible silicate end-member compositions is still sampled.

For a given set of end-members, the constrained solution that minimizes the cost-function need not satisfy the observed mass or charge balance of the river water sample. In other words, it is possible that the products of the model predicted mixing fractions (f_j) and constrained end-member compositions do not exactly match the

river observations. This generic issue affecting most inversion models has various potential solutions, including accepting only a subset of "best-fitting" results (Hemingway et al., 2020; Torres et al., 2016). Here, we avoid poor-fitting parameter combinations by constraining the model to only accept simulations where the predicted values for all solute concentration ratios were within ±20% of observations, predicted δ^{26}Mg, δ^{30}Si, and δ^{44}Ca values were within ±0.2‰ of observations, and predicted $^{87}Sr/^{86}Sr$ was within ±0.002 of observations. In effect, this approach accounts for the analytical uncertainty of the riverine measurements and, as means to cull poor-fitting simulations results, is preferable to accepting a fixed percentage of the best-fitting model results. We performed a sufficient number of simulations to generate either 500 (major elements only) or 200 (isotope constrained) results that matched the above constraints for each river sample. In a set of preliminary experiments, we generated 5,000 isotope-constrained model results for a subset of samples and, by downsampling, verified that 200 results were sufficient for characterizing the posterior distributions.

2.3.5. MEANDIR Analysis and Model Metrics

The calculated mixing fractions (f_j) from MEANDIR are used to calculate the proportion of all weathering-derived cations (i.e., those sourced from both carbonate and silicate dissolution) that are sourced from carbonate weathering (R) where:

$$R = \frac{\Sigma^{\pm}_{carbonate}}{\Sigma^{\pm}_{carbonate} + \Sigma^{\pm}_{silicate}} = \frac{f_{carbonate}}{f_{carbonate} + f_{Na-silicate} + f_{K-silicate} + f_{Ca-silicate} + f_{Mg-silicate}} \quad (4)$$

Because we assume that the silicate and carbonate end-members do not contribute to the SO_4 budget, the calculated values of R only reflect the cation contributions. Following Torres et al. (2016), we report R in units of charge equivalents to match C cycle predictions based on alkalinity fluxes. We note here that R can be calculated for both the gross weathering budget (before clay mineral formation; R_{gross}) and net weathering budget (after clay mineral formation; R_{net}) and that these two measures of R need not be the same. For example, if clays only remove K from solution, which is a cation derived from silicate weathering and not carbonate weathering, then R_{net} will be higher than R_{gross}. This is discussed further in Section 4.3.1.

To characterize the degree of primary mineral incongruence, we combine the model results for the relative contributions from the multiple silicate end-members to determine the composition of the overall silicate end-member. The overall silicate end-member for each simulation is calculated by summing the products of the selected $X/\Sigma^{\pm}$ values for each of the individual silicate end-members and their calculated gross mixing fractions (i.e., the mixing fractions re-normalized to sum to 1). Using Na as an example, the fact that only the Na-silicate end-member contributes to the Na budget and that the value of $Na/\Sigma^{\pm}$ for this end-member is 1 means that the $Na/\Sigma^{\pm}$ of the overall silicate end-member can be calculated from the inversion results as

$$Na/\Sigma^{\pm}_{silicate} = \frac{f_{Na-silicate}}{f_{Na-silicate} + f_{K-silicate} + f_{Ca-silicate} + f_{Mg-silicate}} \quad (5)$$

Analogous equations can be written for the other cations. Again, because we assume that the silicate weathering does not contribute to the SO_4 budget, ratios normalized to $\Sigma^{\pm}$ and Σ^{+} are equivalent for the silicate end-members (i.e., $Na/\Sigma^{\pm}_{silicate}$ calculated from the model can be compared directly with Na/Σ^{+} values measured in basalts). Accordingly, we report all estimates of the composition of the overall silicate end-member as $X/\Sigma^{+}_{silicate}$ values for clarity.

To assess secondary mineral incongruence, we utilize the estimated fraction of the normalization variable taken up into secondary clays (f_{clay}). Alone, this value represents the fraction of the observed concentration of $\Sigma^{\pm}$ that was taken up into secondary phases. So, we re-normalize f_{clay} so that it instead expresses the fraction of gross solute release taken up into secondary phases $\left(F^{\Sigma^{\pm}}_{clay}\right)$ where:

$$F^{\Sigma^{\pm}}_{clay} = \frac{-f_{clay}}{1 - f_{clay}} \quad (6)$$

This equation assumes that the model perfectly reproduces the river observations, but can be adjusted slightly for cases where there is some mismatch between the model predictions and river observations. The value of f_{clay} can

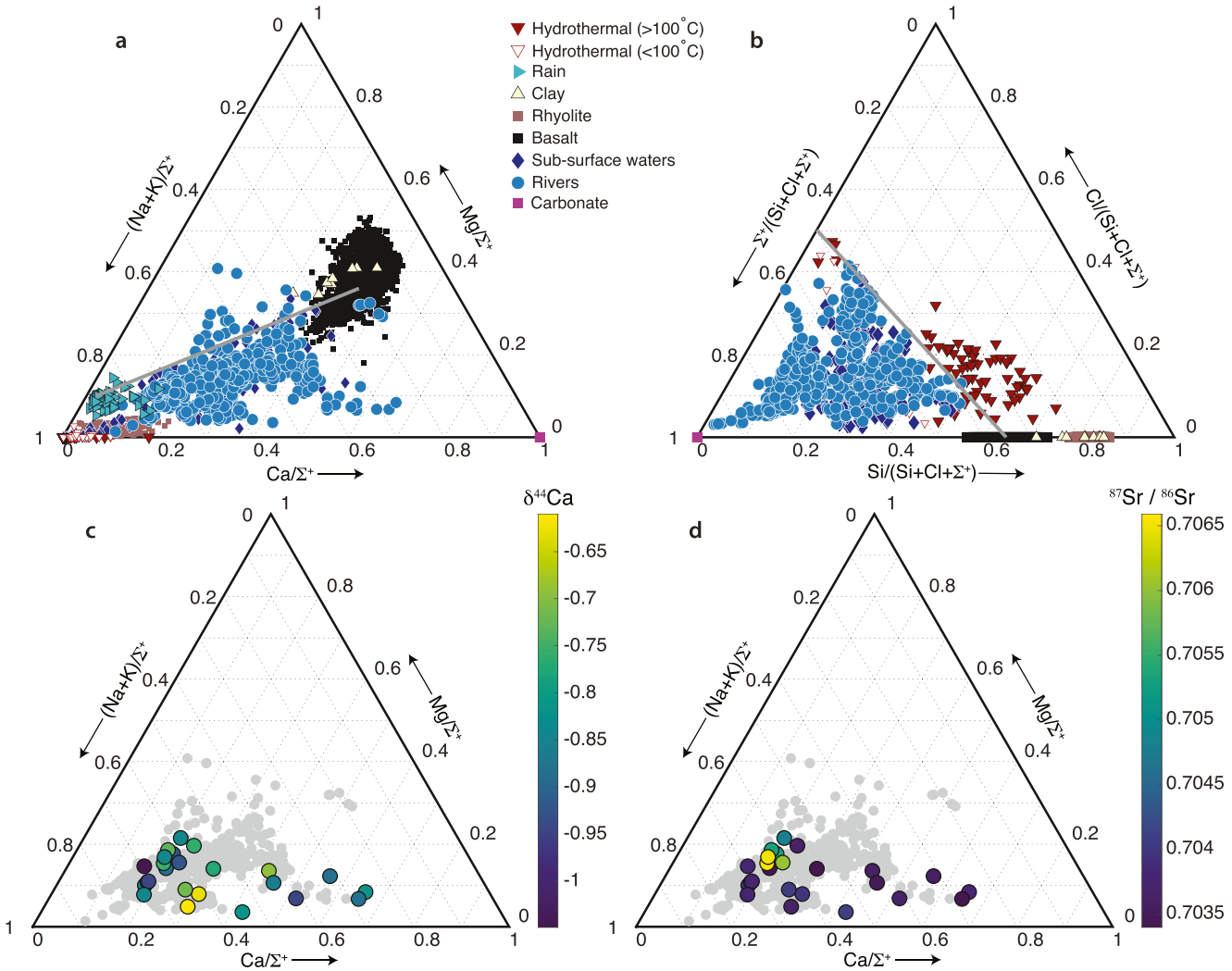

Figure 2. Solid and dissolved phase elemental ratios. (a) Ternary plot showing the proportions of Na + K, Ca, and Mg in river waters (light blue circles), sub-surface waters (dark blue diamonds), rain (light blue triangle), hydrothermal fluids (red triangles), bulk basalts (black squares), bulk rhyolites (light red), clays (yellow triangles), and Ca-carbonates (purple square). (b) Ternary plot showing the proportions of Σ^+, Si, and Cl using the same symbology as panel (a). In both panels a and b, the gray line shows the expected mixing relationship between solutes sourced from basalt dissolution and atmospheric deposition with a seawater composition. (c) Ternary plot showing the proportions of Na + K, Ca, and Mg in the river waters color-coded by δ^{44}Ca (river samples without isotopic measurements are shown in gray). Panel (d) same as in panel (c), but with color-coding by $^{87}Sr/^{86}Sr$.

also be combined with the individual $X/\Sigma^{\pm}$ values for the clay end-member and gross elemental budgets to assess, for each element, the proportion of the gross solute release that was sequestered into secondary phases.

3. Results

3.1. Bedrock Chemistry

Tholeiitic basalts represent ~80% of the compiled database followed by rhyolite (~9%), dacite (3%), trachyte (2%), and to a lesser extent andesite, trachyandesite, trachybasalt, picro basalt and basanite (~6%). This generally matches the areal extent of basalt (80%–85%) and rhyolite (~10%) based on 1:250,000 scale geologic maps (Gíslason et al., 1996; Louvat et al., 2008).

Using the element to sum of major cations (X/Σ^+) normalization, rhyolites and basalts define Na-rich and Ca-rich end-members, respectively (Figure 2). The other rock types (not shown) mostly have intermediate compositions between the rhyolite and basalt end-members, as expected. The values of Na/Σ^+ and Ca/Σ^+ for the culled basalts

range from 0.07 to 0.33 and 0.31–0.55, respectively with mean values of 0.18 and 0.44, respectively. Rhyolite Na/Σ^+ and Ca/Σ^+ values range from 0.444 to 0.767 and 0.007 to 0.247, respectively with an average Na/Σ^+ of 0.62 ($1\sigma = 0.04$).

3.2. Hydrochemical Data Ranges

In the original publications from which our compilation is based, many of the general characteristics of the solute chemistry of natural waters in Iceland were discussed including proposed differences between water types (e.g., glacial vs. non-glacial rivers). For completeness, we re-analyze and re-state some of these observations using our larger data set. While we will primarily focus on the river water samples, various aspects of the other sample types are discussed as they relate to interpreting the river water samples. After quality control (Section 2.1.2), our database includes 96 rain water samples, 32 cold springs samples, 213 glacial river samples, 86 groundwater well samples, 154 hydrothermal fluid samples, 4 lake water samples, 93 multi-sourced river samples, 201 non-glacial river samples, 54 soil pore water samples, and 30 unclassified river samples. Initially, all of the reported concentrations or ratio values will be for samples where no correction for rainwater-derived solutes has been applied. In Section 3.3, we discuss the results of the inverse solute mass balance model, which allows us to correct the data for atmospheric and hydrothermal contributions.

For all of the river water samples, the concentrations of Cl, SO_4, Na, K, Ca, Mg, and Si have median values and ranges (given in parenthesis) of 77 μM (9–1,084 μM), 20 μM (2–2,830 μM), 238 μM (22–2,780 μM), 8 μM (2–225 μM), 109 μM (8–7,780 μM), 58 μM (7–4,330 μM), and 114 μM (20–764 μM), respectively (Figure 3). River water temperatures range between −0.3 and 26°C with a median of 5.2°C. River water pH ranges between 6 and 9.8 with a median of 7.6. The river water samples tend to have higher concentrations of major solutes relative to rain waters (Figure 3), but are generally less concentrated than the sub-surface and hydrothermal waters. The river water samples have a similar, but slightly lower concentration of Cl compared to the monthly rain data, which may reflect contributions from snow/ice melt (Figure 3a). The sub-surface and hydrothermal waters tend to be much more concentrated in Cl relative to the river waters.

With or without removing outliers, a two sample Kolmogorov-Smirnov (K-S) test suggests significant differences in the distributions of solute concentrations, temperature, and pH between glacial and non-glacial rivers with the exception of Na concentrations, which are not significantly different between the two sample types (Figure 3c). In general, glacial river waters are lower in temperature, K, Si, and Cl, but higher in pH, Ca, and SO_4 relative to the non-glacial rivers (Figure 3). While glacial versus non-glacial rivers may reflect different data distributions, these distributions substantially overlap with each other for all measured properties (Figure 3).

When normalizing the river water data by sum of major cations (Σ^+), the ratios Na/Σ^+, K/Σ^+, Ca/Σ^+, Mg/Σ^+, Si/Σ^+, and Cl/Σ^+ have median values and ranges (given in parenthesis) of 0.55 (0.17–0.87), 0.02 (0.004–0.13), 0.26 (0.09–0.66), 0.15 (0.01–0.41), 0.27 (0.01–1.28), and 0.20 (0.03–0.87), respectively. These ranges do not exactly match what is observed in bulk basalts from the GEOROC database (Figure 2). In general, the river water data un-corrected for rainwater inputs are enriched in Na/Σ^+ or, conversely, depleted in Mg/Σ^+ relative to bulk basalts (Figure 2a). Similar discrepancies are observed for the sub-surface water samples (Figure 2). As with the concentration data, a K-S test suggests significant differences in the distributions of elemental ratios between glacial and non-glacial samples with the exception of Na/Σ^+, which does not appear to have a significantly different distribution between the two river types. Relative to the non-glacial rivers, glacial rivers generally have higher Ca/Σ^+ values, but lower K/Σ^+, Mg/Σ^+, Si/Σ^+, and Cl/Σ^+ values.

Atmospheric deposition and hydrothermal fluids are the only end-member water types that can contribute Cl to rivers. Most of the rain samples have Cl/Σ^+ values near 1 whereas hydrothermal fluids show lower and more variable Cl/Σ^+ values (Figure 2b). Both the rain water and hydrothermal fluid samples show elevated Na/Σ^+ values close to the seawater ratio of 0.86 (Figure 2b). Both the river and sub-surface waters are depleted in Si/Σ^+ relative to basalts, rhyolites, and hydrothermal fluids (Figure 2b).

3.3. Source and Sink Apportionment

Our solute mass balance model was able to reproduce all of the quality-controlled river water samples with valid mixing fractions with or without the added isotopic constraints. In Figures S2–S5 of Supporting Information S1,

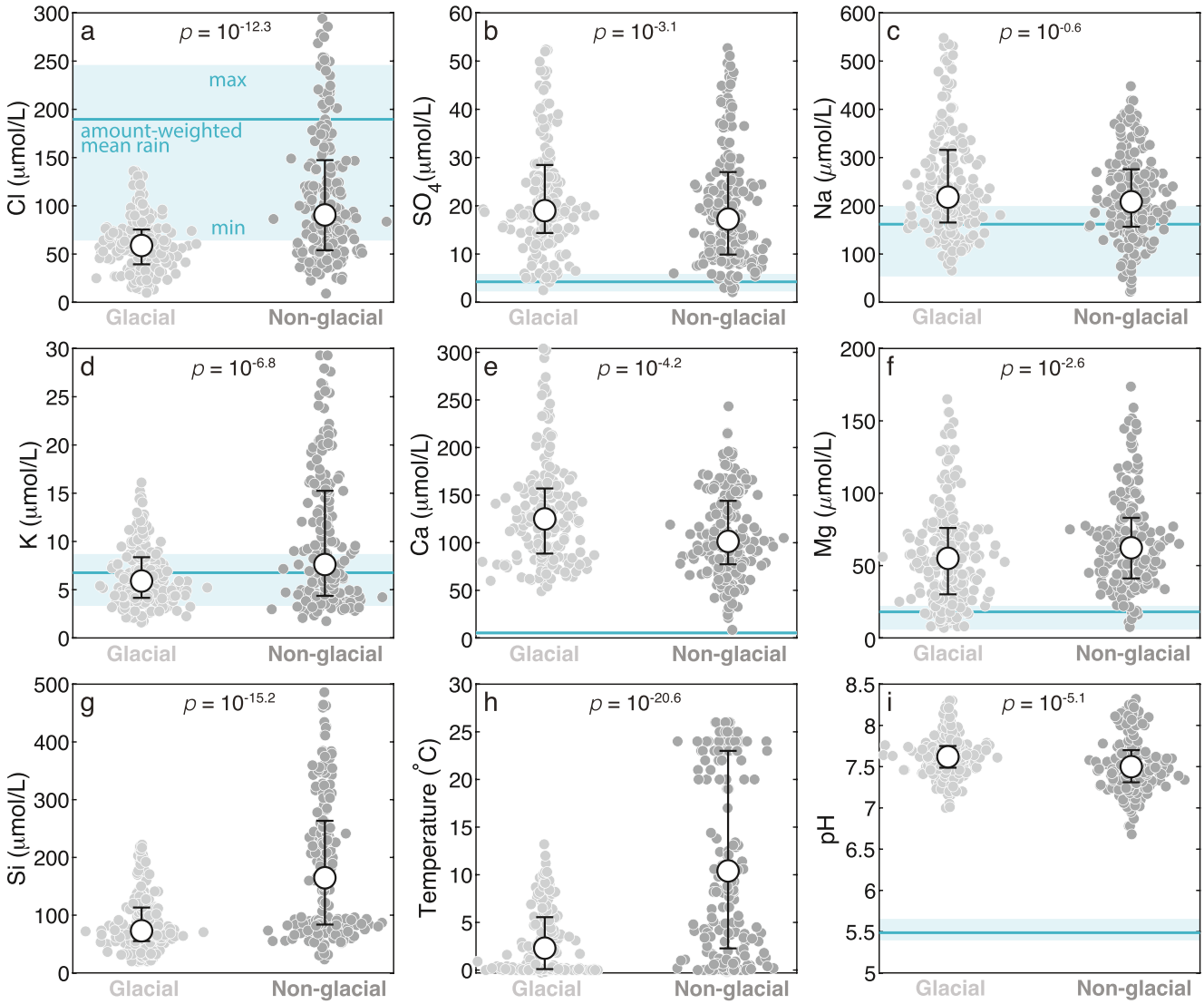

Figure 3. Jitter plots of solute concentrations, temperature, and pH for glacial (light gray) and non-glacial (dark gray) river waters. The white points with black outlines indicate the median value for each data distribution and the range from the 25th to 75th percentiles of the data. Outliers from all data distributions have been removed for visualization and do not affect the outcomes of the Kolmogorov-Smirnov test used to asses differences between the data distributions (associated p values are listed in each panel). The solid blue lines show the amount weighted mean values for rainwater from the Íráfoss site. The light blue rectangles show the range from the minimum to maximum rainwater values for each parameter. No rainwater values are shown for Si concentration (panel g) or temperature (panel h).

we show the reconstructed river values for a subset of samples with Mg, Si, Ca, and Sr isotopic ratios, which provides an assessment of how accurately the mixing fractions reproduce the observations. In Figure S6 of Supporting Information S1, we show an example of how the slight model-data mismatches allowed in our analysis (see Section 2.3.4) do not impact our results using the reconstructed value of $^{87}Sr/^{86}Sr$ and the predicted proportion of carbonate weathering (R_{net}) as an example.

As we set our model to find up to 200 or 500 valid model results for each sample, each derived parameter, such as the net ratio of carbonate-derived cations to the sum of carbonate and silicate derived cations (R_{net}; Equation 4) is best described as a distribution of values (Figure 4). The exact shape of this distribution can be sensitive to the distributions used to draw end-member ratios and the applied simulation acceptance criteria. As a result, the mean, median, or modal results need not be closer to the "true" value relative to some of the rarer results. To describe the distributions of model output variables, we calculate the 5th, 25th, 50th, 75th, 95th, and 99th percentiles of the model results for each sample.

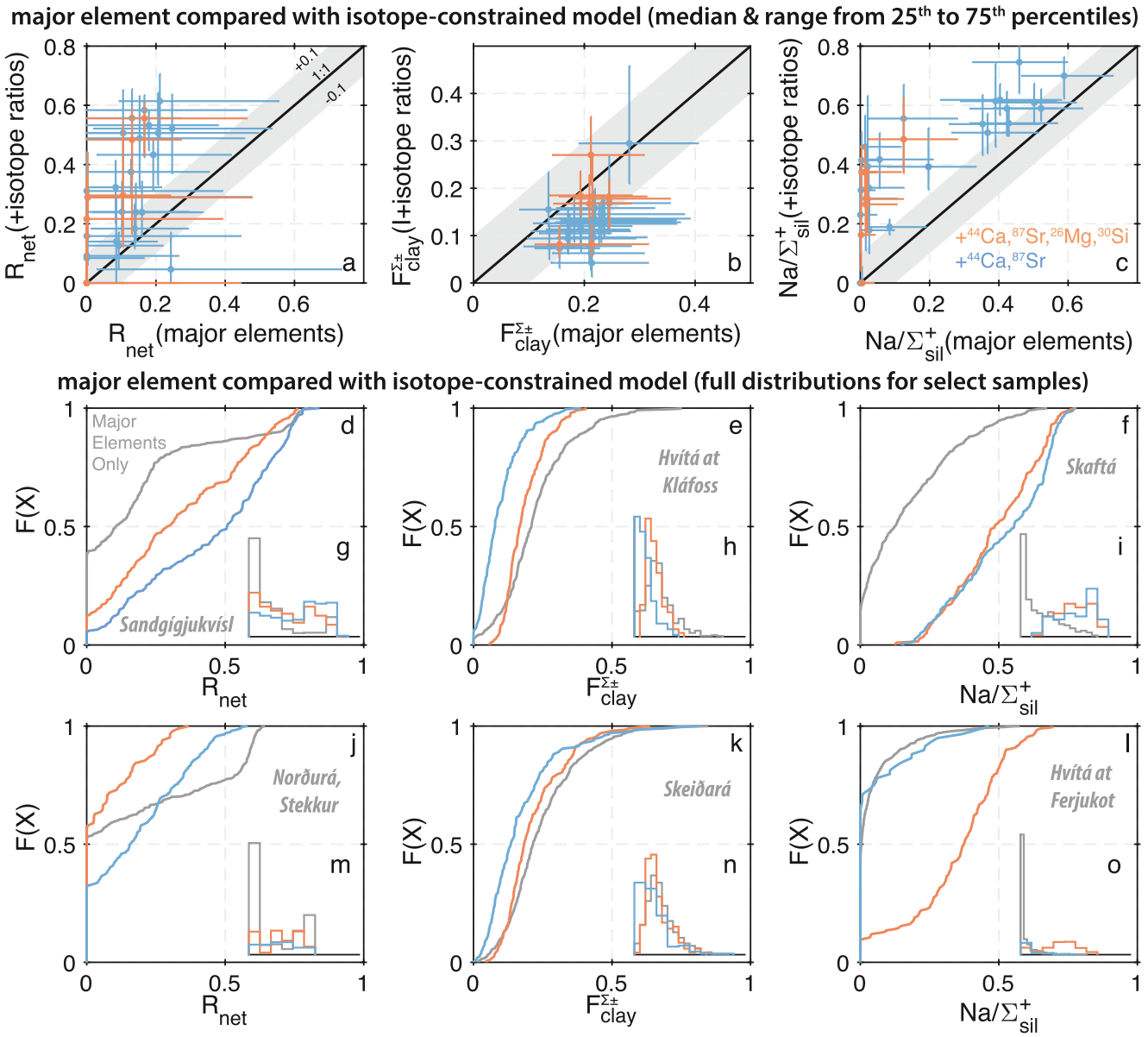

Figure 4. Comparison of solute mass balance model results with and without added isotopic constraints. Panels (a–c) compare the median (point) and 25th to 75th percentile range (error bar) results calculated using major elements only (*x*-axis) with the results calculated using added isotopic constraints for the proportion of carbonate weathering (R_{net}; Equation 4; panel [a]), the fraction of solute uptake into clay ($F^{\pm}_{clay}$; Equation 6; panel [b]), and the Na/Σ^+ of the silicate end-member (Equation 5; panel c). For the results using isotopic constraints, we show the 24 samples with Ca and Sr isotopic data in blue. Seven of these 24 samples have additional measurements of Mg and Si isotopic ratios, so we show the inversion results using all four isotopic ratios in orange. The black line in the panel shows a 1:1 relationship with the gray shading showing ±0.1. Panels (d–o) show full intra-sample distributions for the three model parameters using six individual rivers (Grimsá River not shown) where either major elements (gray), Ca and Sr isotopic ratios (solid blue), or Mg, Si, Ca, and Sr isotopic ratios (solid orange) are used as model constraints. The main panels show cumulative distribution functions (panels d–f and j–l) and the inset panels show probability density functions (panels g–i and m–o).

The *a priori* range of possible values span a known interval for all of the derived parameters we constrain with our model (i.e., R_{net} can only range between 0 and 1). Therefore, the model provides new information when the range of results it returns spans a smaller range than the *a priori* range. For the parameters we investigate, which include R_{net}, the proportion of gross cation supply incorporated into clays $\left(F^{\Sigma^+}_{clay}\right)$, and the degree of primary mineral congruence, the model returns distributions that span narrower ranges than what is allowable and, as a result, these parameters are constrained by the model.

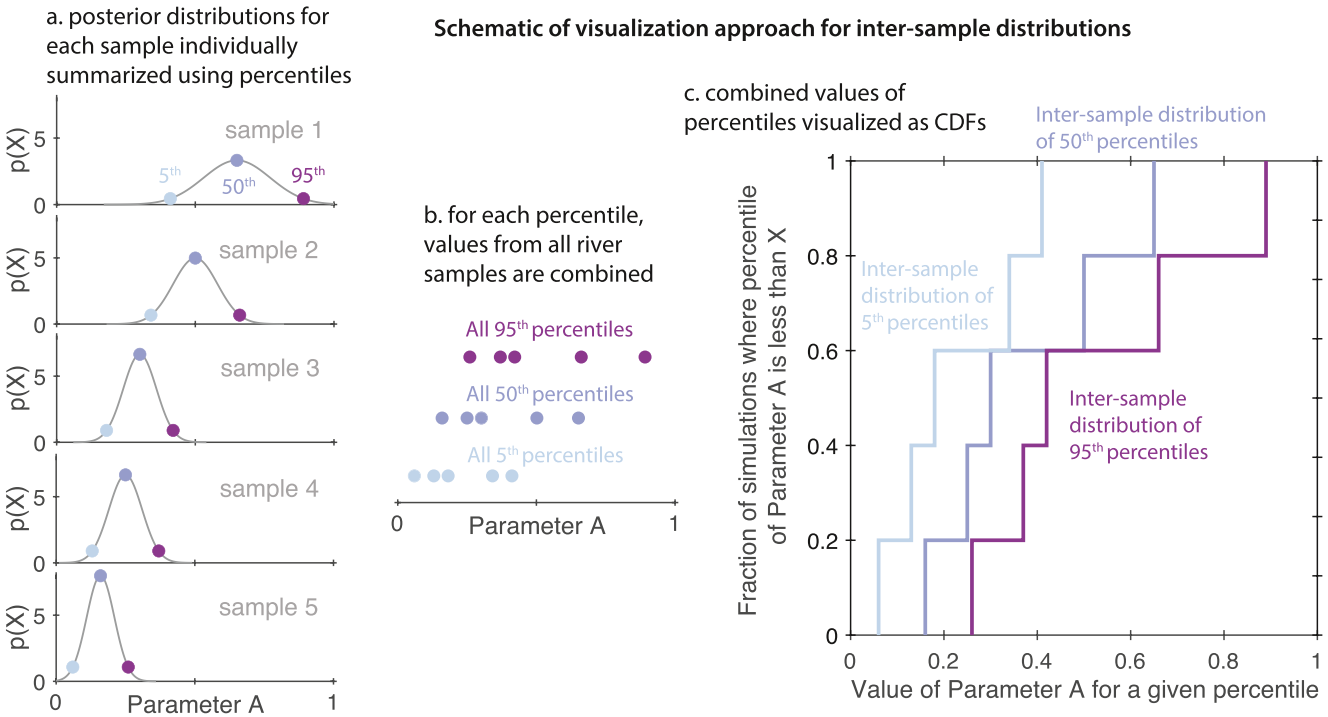

Figure 5. Schematic showing how inter-sample distributions of percentiles are calculated from the individual sample distributions.

In addition to looking at the distributions of model parameters at the level of individual samples, we also look at the ranges of for each percentile across all samples. For example, we calculate the 5th percentile of $F_{clay}^{\Sigma+}$ for each sample and then look at the distribution of the pooled 5th percentile values. This approach of looking at the inter-sample distribution of a percentile value emphasizes the range of a particular statistic across all samples. In Figure 5, we show a schematic of our approach to visualizing the model results as inter-sample distributions of percentiles.

3.3.1. Predicted Isotopic Fractionation

While isotopic data are only available for a small subset of our full data set, they can offer important insights into the interpretation of the results derived using only major element concentrations as model constraints (Section 2.3). However, the degree to which the inversion model is constrained by including isotopic data depends on knowledge of fractionation factors for the incorporation of elements into secondary minerals. Given limited direct measurements and/or experimental constraints (Section 2.3.3), we opted to include a wide range of values for a prior distributions of Mg, Si, and Ca fractionation factors (Equation 3). Using the posterior distributions of fractionation factors for each isotopic system, we can assess the model performance as, in some cases, values at the extreme ends of our prior distributions may be less likely and/or associated with specific processes or secondary mineral phases.

For Si isotopic ratios, all samples can be modeled with a negative fractionation factor (Δ^{30}Si), which is the expectation for clay formation (Figure 6a; Baronas et al., 2020; Cornelis et al., 2014; Ziegler, Chadwick, Brzezinski, & Kelly, 2005). Four out of the seven samples can be described by Δ^{30}Si greater than or equal to zero, which is the expectation for amorphous Si (Roerdink et al., 2015; Zheng et al., 2019). Similarly, For Mg isotopic ratios, all of the samples can be modeled with negative fractionation factors (Figure 6b), which is the expectation for smectite-group clays (Hindshaw et al., 2020). As with Si, $\Delta^{26}\text{Mg} \geq 0$ is allowable for three out of the seven samples.

Unlike for Si and Mg isotopic ratios, the posterior distributions of Δ^{44}Ca values span nearly the same range as the prior distributions (Figure 6c). So, both positive and negative Ca isotopic fractionations are allowable. Similarly, all of the data can be modeled assuming that secondary phases do not fractionate Ca isotopic ratios (i.e., $\Delta^{44}\text{Ca} = 0$). Given that both carbonate dissolution and secondary phase formation with a negative Δ^{44}Ca value

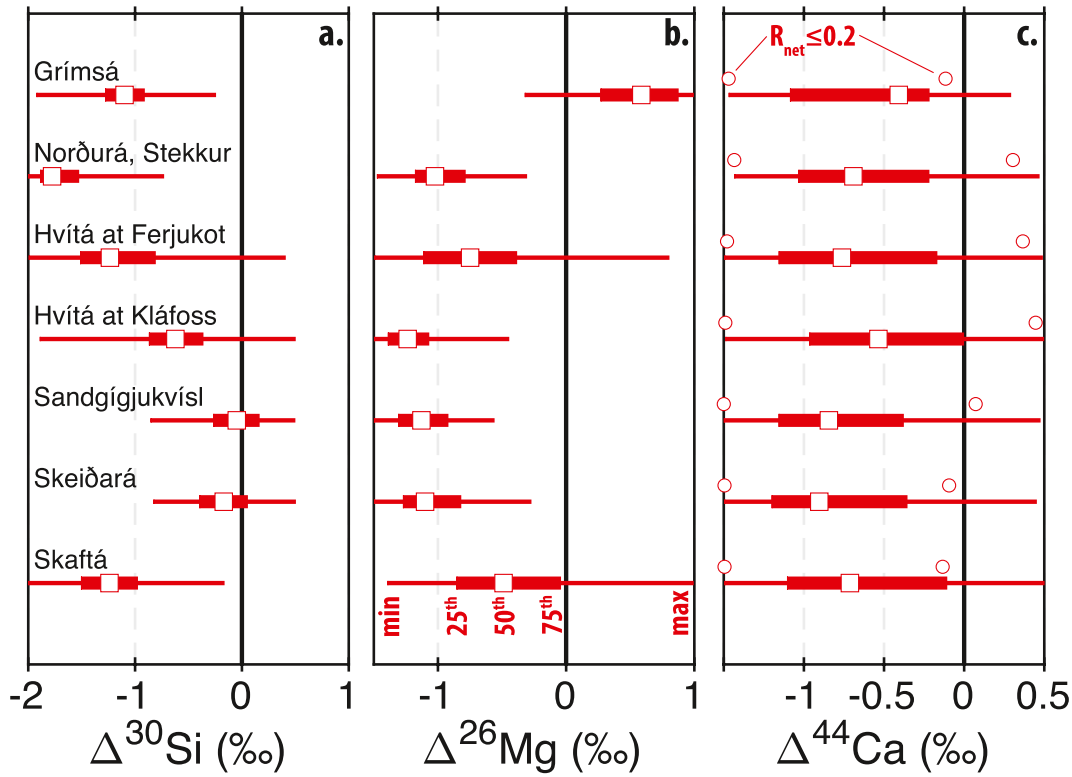

Figure 6. Inversion-constrained fractionation factors (Equation 3) for Si (panel a), Mg (panel b) and Ca (panel c) isotopic ratios. In each panel, the *x*-axis scale spans the range of the prior distribution for each isotopic system. For each sample, the range from minimum to maximum allowable fractionation factor is shown as the thin bar. The thick bar shows the range from the 25th to 75th percentiles. The white square shows the median result. In panel (c), the circles show that minimum to maximum range in Δ^{44}Ca for each sample for the subset of simulations where the proportion of carbonate weathering (R_{net}) is less than 0.2.

would tend to increase riverine δ^{44}Ca (Hindshaw et al., 2013; Jacobson et al., 2015), it is reasonable to expect a trade-off where simulations with lower proportions of carbonate weathering (R_{net}) are associated with lower Δ^{44}Ca values and vice versa. Such a trade-off would be important to recognize as the limited experimental data for freshwater systems suggest Δ^{44}Ca values of −0.1 to −0.3 ‰ (Brazier et al., 2019; Hindshaw et al., 2013) rather than values closer to the lower bound of our prior distribution, which is informed by experiments conducted at high ionic strength (Ockert et al., 2013) and the range of global riverine Ca isotopic measurements (Bouchez et al., 2013). With this in mind, we report the range of Δ^{44}Ca values for the subset of simulations in each sample where R_{net} is less than or equal to 0.2 (i.e., no more than 20% of the sum of carbonate and silicate alkalinity is derived from carbonate weathering in units of charge equivalents). While this range is shifted to lower Δ^{44}Ca values relative to the full range of model simulations (Figure 6c), there are still simulations for each sample where Δ^{44}Ca values are entirely compatible with known Ca isotopic fractionation factors for adsorption onto clay surfaces in freshwater (Brazier et al., 2019). So, while our data can be modeled with large, negative Δ^{44}Ca values, such values are not necessary to reproduce the observations even when assuming low contributions from carbonate weathering.

3.3.2. Comparison Between Results With and Without Added Isotopic Constraints

Given the ability of our model to fit all of the river samples with isotopic measurements using reasonable values for Mg, Si, and Ca fractionation factors (Figure 6), we can compare the results obtained using isotopic constraints to those obtained using only major element data for the same sample set (Figure 4). The purpose of this comparison is to identify whether or not including isotopic data substantially modifies the model results for the proportion of carbonate weathering (R_{net}), the fraction of gross solute supply taken up into secondary clays $\left(F^{\pm}_{clay}\right)$ and the overall composition of the silicate end-member $\left(\mathrm{Na}/\Sigma^{+}_{sil}\right)$. Ultimately, identifying any systematic differences will

help us to better interpret the model results for the majority of samples where only major element data are available. We note, however, that the river samples with isotopic data do not span the full range of geochemical variability observed for all rivers in Iceland (Figures 2c and 2d). Specifically, Mg- and Ca-rich river water samples similar in composition to bulk Icelandic basalts have not been characterized for their Mg, Si, Ca, or Sr isotopic compositions (Figures 2c and 2d).

For our estimates of R_{net}, the median results using isotopic constraints tend to be higher than the results using only major elements constraints (Figure 4a). However, in most cases, the 25th to 75th percentile ranges of R_{net} values overlap for the model results with and without isotopic constraints (Figure 4a). In other words, the upper and lower bounds tend to be similar with and without isotopic constraints, but, within those bounds, the shape of the distribution can be substantially different (Figures 4a, 4d, 4g, 4j, and 4m).

For $F_{clay}^{\Sigma+}$, including isotopic constraints tends to decrease the median values for most samples (Figure 4b). In some cases, the upper bound on $F_{clay}^{\Sigma+}$ markedly decreases when isotopic constraints are included (e.g., Figures 4e and 4h). Accordingly, adding isotopic constraints appears to help to bound the role of cation uptake into clays. As such, the highest values of $F_{clay}^{\Sigma+}$ predicted for a sample using only major elements as constraints is likely an over-estimate for this parameter.

For Na/Σ_{sil}^{+}, added isotopic constraints slightly increases the median values for most samples (Figure 4c). Given the changes in both $F_{clay}^{\Sigma+}$ and Na/Σ_{sil}^{+}, including isotopic constraints tends to favor results where there is relatively less secondary mineral incongruence and relatively more primary mineral incongruence (Figures 4b and 4c). For the sample set we test (Figures 2c and 2d), using $\delta^{26}Mg$ and $\delta^{30}Si$ as added constraints does not substantially change the distribution of model results relative to using just $\delta^{44}Ca$ and $^{87}Sr/^{86}Sr$ (e.g., Figures 4d, 4f, and 4k), but slight differences are apparent for some samples (e.g., Figures 4j and 4l).

While there are coherent differences in median values of R_{net}, $F_{clay}^{\pm}$, and Na/Σ_{sil}^{+} with and without the added constraints from isotopic ratios (Figures 4a–4c), the different distributions tend to show very similar ranges for a given sample (e.g., Figures 4d and 4k). Therefore, it is likely reasonable to use the major element only version of the model to place upper and/or lower bounds on the model parameters for each sample. While the major element only model can overestimate the upper bound on $F_{clay}^{\Sigma+}$ (e.g., Figure 4e), the differences between the model results and without isotopic constraints vary by about 0.1 (Figure 4b), which provides some guidance for how precisely the results can be interpreted. For Na/Σ_{sil}^{+}, the observation that the major element only model tends to under-predict this ratio (Figure 4c) suggests that the upper bound calculated using major elements alone is a conservative estimate.

4. Discussion

Conservative mixing between solutes sourced from congruent basalt dissolution and atmospheric deposition fails to explain a majority of the river and sub-surface water data from Iceland (Figure 2; Gíslason et al., 1996). Multiple competing mechanisms exist to explain the discrepancy between this *null* hypothesis for basaltic watersheds and the observations from Iceland. The uptake of cations in secondary clays (secondary phase incongruence; Gíslason et al., 1996; Hindshaw et al., 2013; Moulton et al., 2000; Stefánsson et al., 2001), the dissolution of rhyolites (Louvat et al., 2008), and the dissolution of hydrothermal calcite (Andrews & Jacobson, 2017; Georg et al., 2007; Jacobson et al., 2015) have all been proposed as additional factors that influence the chemical composition of Icelandic rivers. Here, we also consider the potential for the silicate end-member to be characterized by different elemental ratios compared to bulk igneous rocks (primary mineral incongruence).

As detailed below, we find evidence that both primary and secondary mineral incongruence contribute to observed chemical composition of Icelandic rivers. Carbonate weathering is not strictly required by any of the river water samples in our database, but carbonate contributions are permissible in all samples. In order for carbonate weathering to contribute more to the total cation budget, the relative importance of incongruent weathering must be increased. Below, we describe the evidence for each of these findings, discuss the apparent differences between water sample types (i.e., glacial vs. non-glacial and river vs. sub-surface), and provide potential mechanisms underlying the apparently incongruent weathering taking place in Iceland.

4.1. Evidence for Cation Uptake by Secondary Phases (Secondary Phase Incongruence)

A majority of the river water samples are relatively depleted in Mg, K, and Si relative to what would be expected from conservative mixing between solutes sourced from congruent basalt dissolution and atmospheric deposition (Figures 2a and 2b). Interpreting this to reflect some uptake of Si, Mg, and K into secondary clays is consistent with calculations of super-saturation with respect to various clay minerals (Georg et al., 2007; Hindshaw et al., 2013, Figure S7 and Supporting Information S1) as well as available measurements of fine-grained sediments in Iceland, which can be enriched in Si, Mg, and K relative to bulk basalts (Figures 2a and 2b; Moulton et al., 2000; Thorpe et al., 2019). Selectively removing a specific cation or set of cations affects all element to $\Sigma^{\pm}$ ratios by modifying the denominator term. Assuming clays do not take up much Na, which is consistent with the available sediment measurements (Figure 2; Moulton et al., 2000; Thorpe et al., 2019), clay formation would act to increase Na/Σ^{+} relative to what is expected for basalt dissolution and atmospheric deposition, which is observed (Figure 2a).

The extent of Mg-depletion and Na-enrichment could also be due to contributions from hydrothermal fluids (Figure 2a), though this would not explain the observed extent of Si depletion as most hydrothermal fluids have high Si/Σ^{+} (Figure 2b) even after allowing for potential Si loss during cooling (Geilert et al., 2015). Additionally, our isotope-constrained mixing model predicts the gross contribution of hydrothermal fluids to the $\Sigma^{+}+SO_4$ budget to be less 20% using the median values for 22 of the 24 samples constrained with Ca and Sr isotopic ratios (the Sandgígjukvísl and Grimsá River have higher median hydrothermal contributions of 31% and 43%, respectively).

The uptake of cations into clay minerals in Icelandic watersheds has been suggested previously using the concentrations and isotopic compositions of both major and trace elements in both the solid and dissolved phase (Ehlmann et al., 2012; Georg et al., 2007; Gíslason et al., 1996; Hindshaw et al., 2013; Moulton et al., 2000; Pogge von Strandmann et al., 2006; Stefánsson et al., 2001; Thorpe et al., 2019; Vigier et al., 2009). Nevertheless, the magnitude of cation uptake remains poorly constrained. Using the solute mass balance, we refine estimates of clay cation uptake for all of the samples with major element data. Importantly, differences between the MEANDIR model results with and without isotopic constraints suggest that the major element only version of the model slightly over-estimates the maximum allowable amount of cation uptake into clays (Figures 4f and 4l). We account for this by using the 95th percentile for each sample distribution as an estimate of the upper bound for each sample. Since every sample has a different 95th percentile value, the variability in this statistic between samples can be described using an inter-sample distribution (a schematic explanation of inter-sample distributions is shown in Figure 5).

Using the inter-sample distribution of 95th percentiles, we find that, for a majority (i.e., 60%) of samples, no more than ~60% of the cations released by weathering (or provided by atmospheric deposition and/or hydrothermal fluid discharge) are taken up into secondary clays (Figure 7a). Looking at the inter-sample distribution of 5th percentiles, a few samples allow for zero cation uptake into clays whereas others require, at a minimum, ~10% of the total cation supply to have been sequestered into secondary clays (see upper bound of 5^{th} percentile curve in Figure 7a). For Mg and K, clay formation tends to account for a larger proportion of the gross solute release compared to Na and Ca (Figures 7b–7e). The distribution of 95th percentile values suggest that, for most (60%) samples, up to roughly 26%, 95%, 67%, 81%, and 95% of Na, K, Ca, Mg, and Si are taken up to clays, respectively (Figures 7b–7f). Using the distribution of median values, most samples suggest that up to roughly 6%, 81%, 30%, 45%, 90% of Na, K, Ca, Mg, and Si are taken up to secondary clays, respectively (Figures 7b–7f).

4.2. Evidence for Preferential Na Release From Silicates (Primary Mineral Incongruent Weathering)

While clay mineral formation acts to increase riverine Na/Σ^{+}, it is likely insufficient to explain the full extent of Na enrichment evident in the river water data. In part, this is because the magnitude of cation uptake into clays is limited by the Si budget (Figure 7f) and the relatively low Σ^{+}/Si ratios of measured Icelandic clays (Figure 2b). While contributions from atmospheric deposition and/or hydrothermal fluids also act to increase Na/Σ^{+}, this mechanism cannot explain the high Na/Σ^{+} values observed for river samples with relatively low Cl/Σ^{+} (Figure 2b). To explore alternative mechanisms, we utilize our reconstruction of the overall silicate end-member from the four individual components (Equation 5).

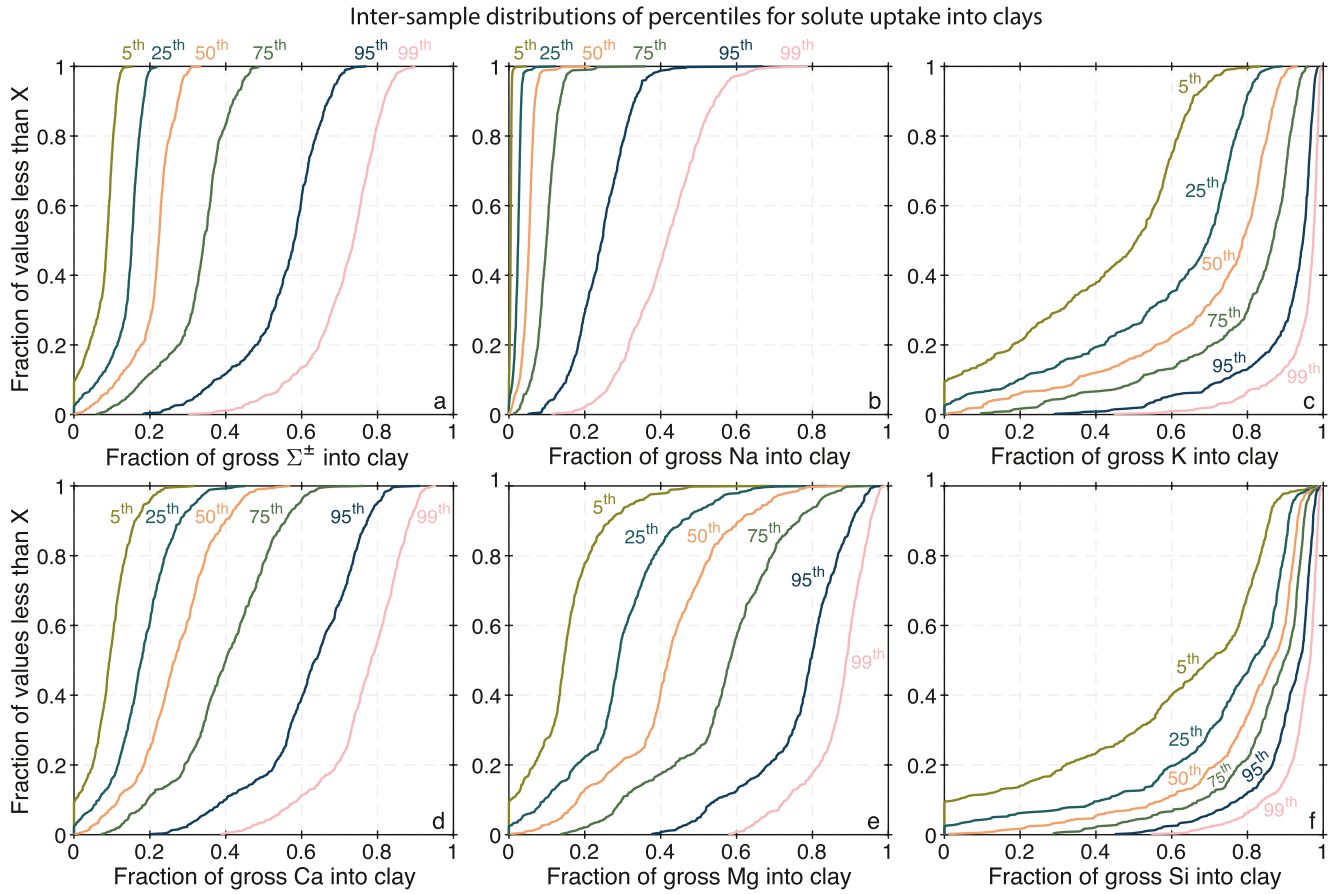

Figure 7. Fractions of gross solute release sequestered into secondary clays. Each panel shows the inter-sample variability (as an empirical cumulative distribution function) in the 5th, 25th, 50th, 75th, 95th, and 99th percentiles calculated from the 500 simulations for each sample. For example, the blue curve labeled "95th" in panel a shows the range in the 95th percentile of the fraction of gross Σ^+ sequestered into secondary clay calculated from each individual sample. Panels (a–d) show the fraction of the gross amount of Σ^+, Na, K, Ca, Mg, and Si sourced to each sample that was sequestered into secondary clays, respectively.

For many river water samples, the calculated overall silicate end-member using the default model does not match the (Na + K)/Σ^+, Ca/Σ^+, and Mg/Σ^+ values observed for bulk basalts in the GEOROC database (Figure 8). Instead, the model returns an overall silicate end-member that is relatively depleted in Ca and enriched in Na compared to bulk basalts (Figure 8). The visualization in Figure 8a shows the calculated silicate end-member compositions for all of the river water samples using only major elements as model constraints. For clarity, results where Na/Σ^+_{sil}, Ca/Σ^+_{sil}, or Mg/Σ^+_{sil} were less than 0.01 or K/Σ^+_{sil} was less than 0.001 were filtered out. By grouping all of the data together, we highlight silicate end-member compositions that are shared by the most samples. The modal result in Figure 8a is outside of the 1st to 99th percentile range of basaltic compositions and falls along the mixing trend from basaltic to rhyolitic rock compositions.

While Figure 8a emphasizes end-member compositions that are shared between river samples, it is also the case that different river samples are characterized by different silicate end-member compositions. In Figure 8b, we show the 5th to 95th percentile results for the inversion constrained Na/Σ^+ value for the silicate end-member using the 24 samples with Ca and Sr isotopic constraints. In nine of these samples, Na/Σ^+_{sil} is higher than bulk Icelandic basalts (Figure 8b). In contrast, only 4 samples return model results that only match basaltic Na/Σ^+_{sil} values (Figure 8b). The remaining 11 samples can be fit by either a basaltic or rhyolitic Na/Σ^+_{sil} value (Figure 8b).

4.2.1. Potential Mechanisms of Preferential Na Release During Silicate Weathering

Roughly 10% of Iceland is underlain by rhyolitic bedrock (Gíslason et al., 1996; Louvat et al., 2008), fine-grained rhyolitic tephra is deposited on catchment surfaces by local volcanic eruptions (Larsen & Eiriksson, 2008; Óskarsson et al., 2012), rhyolitic glass can be present as an interstitial phase in basalts (Meyer & Sigurdsson, 1978)

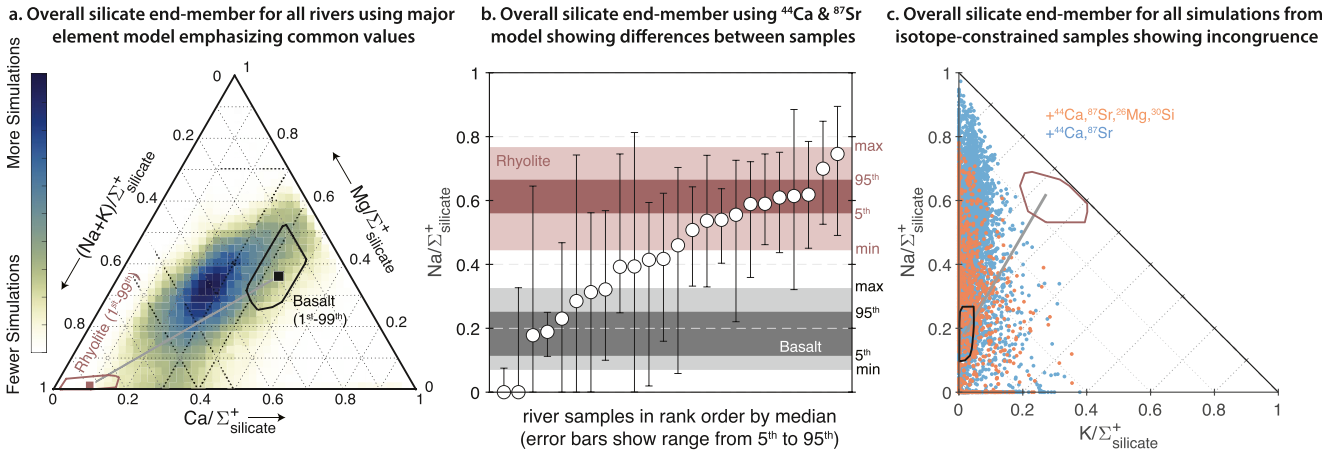

Figure 8. Inversion constrained composition of the silicate end-member. (a) Ternary diagram of the proportions of Na + K, Ca, and Mg. The MEANDIR results using only major element data are represented as a 2D histogram where darker colors reflect more simulations from each sample producing an end-member composition with that particular value. For comparison, we show the compositions of basalts and rhyolites as black and light red squares with outlines that encompass 98% of the measured variability. The gray line connecting the black and light red squares is the mixing line between mean basalt and mean rhyolite. (b) Inversion constrained values for the Na/Σ^+ using Ca and Sr isotopic data as model constraints. The white circles show the median values calculated using the model and the error bars show the range from the 5th to 95th percentiles. For comparison, we show the minimum/maximum (light shading) and 5^{th}/95th percentile (dark shading) ranges of Na/Σ^+ for Icelandic basalts (black) and rhyolites (light red). (c) Incongruent release of Na relative to K evident in the isotope-constrained solute mass balance model simulations. The blue (Ca and Sr isotope constrained; $n = 24$) and orange (Mg, Si, Ca, and Sr isotope constraints; $n = 7$) points show the predicted composition of the silicate end-member for each individual simulation for all rivers considered. Similar results (i.e., incongruent release of Na relative to K) are also obtained using only major elements as constraints.

and, in laboratory experiments, rhyolitic glass dissolves as fast as crystalline basalt (Wolff-Boenisch et al., 2004). Similarly, basalts contain albite ($NaAlSi_3O_8$) as a major phase and laboratory experiments are consistent with albite dissolution rates matching the dissolution rate of anorthite ($CaAl_2Si_2O_8$) at circum-neutral pH values after surface area normalization (Brantley et al., 2008). It follows that some contribution from the weathering of Na-rich lithologies and/or minerals could explain the general enrichment in Na/Σ^+ of the overall silicate end-member determined from the river water data (Figure 8).

If the Na-enrichment of the silicate end-member is due to the preferential weathering of interstitial rhyolitic glass or albite in basalts, then it can reasonably be classified as primary mineral incongruence. If instead it derives from the weathering of rhyolite outcrops or ash deposits (Louvat et al., 2008), then it is more appropriately thought of as multiple silicate end-members. Some model results do not produce a silicate end-member that exactly matches mixing between bulk basalts and bulk rhyolites (Figures 8a, 8c, and 9b). Instead, the calculated silicate end-members can be K-poor (Figure 8c) or Ca-rich (Figure 9b) relative to expectations for contributions from congruent rhyolite dissolution and basalt weathering. As such, even if the Na-enrichment is due to the dissolution of rhyolitic outcrops or ash deposits, the weathering of this more felsic material is characterized by primary mineral incongruence, especially with respect to K (Figure 8c).

Ultimately, classifying the observed silicate end-member as resulting from primary mineral incongruence versus multiple silicate end-members is important as the exact mechanism(s) underlying the dissolved Na enrichment of Icelandic watersheds, which persists after clay formation, atmospheric deposition, or hydrothermal fluid discharge are taken into account, underlies the applicability of studies from Iceland to other volcanic systems (Börker et al., 2019). Future work looking at the compositions of soils, fluvial sediment, and weathered rocks may provide helpful constraints to address this knowledge gap.

4.3. Constraints on Carbonate Contributions to Icelandic Rivers

The dissolution of trace calcite formed during the hydrothermal alteration of basalts could potentially contribute some proportion of the total Ca measured in Icelandic rivers (Andrews & Jacobson, 2017; Georg et al., 2007; Jacobson et al., 2015). Given the overall trend of Na enrichment in Icelandic rivers (Figure 2a), contributions from carbonate weathering alone cannot explain the data without also including incongruence. Nevertheless, the

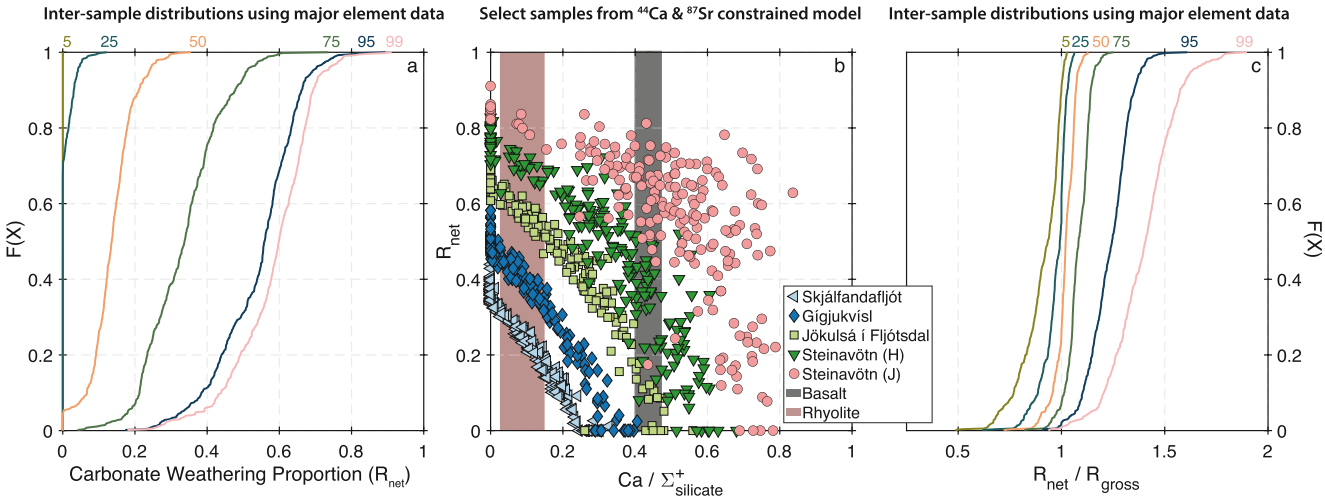

Figure 9. Constraints on carbonate contributions from the solute mass balance model. (a) Empirical cumulative distribution functions of the inter-sample variability in the 5th, 25th, 50th, 75th, 95th, and 99th percentiles of the carbonate weathering proportion (R_{net}; Equation 4). (b) The values for the Ca/Σ^+ of the silicate end member and R_{net} for individual simulations for a subset of 5 samples with Ca and Sr isotopic constraints. Each point is a single simulation and the different colors correspond to different river water samples. The ranges of Ca/Σ^+ for basalts and rhyolites from the GEOROC database are shown as black and salmon rectangles, respectively. (c) The ratio of net carbonate contributions to gross carbonate contributions calculated from the inversion of major element data only shown as an inter-sample distribution of percentiles.

C cycling implications of carbonate weathering are very different than silicate weathering, so it is important to determine what proportion of the cation budget may be derived from carbonates.

The model results for R_{net} imply that the dissolution of carbonate is not required to explain the elemental and isotopic composition of Icelandic rivers (Figure 9a). Specifically, using the 5th percentile of R_{net} as a guide for the minimum carbonate contribution, the largest value we find for any river sample is 0.0004% and thus represents a negligible contribution from carbonate dissolution. Using the 95th percentile of the range of model results for each sample, most samples are incompatible with substantial carbonate contributions as a minority (<40%) of samples yield inversion results where >60% of the cation budget derives from carbonate weathering (Figure 9a). The few samples that are suggestive of large carbonate contributions are characterized by distinctly low Na/Σ^+ and high Ca/Σ^+ values relative to most of the other river water data. However, for these same samples, model solutions with low values of R_{net} that match elemental and isotopic constraints are also found where the solution chemistry is explained by the preferential release of Ca from silicate minerals (Figure 9b).

Considering all samples together, the aggregate distribution of R_{net} can be interpreted as having two modes (e.g., Figures 4d and 9b): one with a low carbonate contribution ($R_{net} < 0.1$) and one with a higher carbonate contribution ($R_{net} > 0.5$). This results from a trade-off between the degree of primary mineral incongruence and carbonate contributions (Figure 9b). In order to get high values of R_{net}, it is necessary to have a silicate end-member that is more depleted in Ca relative to bulk basalts (Figure 9b).

This trade-off between the composition of the overall silicate end-member and the proportion of cations from carbonate weathering reflects the ambiguity of our selected tracers. To improve estimates, we consider two approaches and apply them to the subset of the data where it is currently possible. Both of these approaches act to decrease the amount of carbonate weathering allowable in each sample. Accordingly, we posit that silicate weathering dominates the alkalinity budget of chemical weathering in Iceland.

One additional tracer useful for constraining R_{net} is the normalized ^{14}C content (percent modern carbon; pMC) of dissolved inorganic carbon (DIC). This is because the dissolution of hydrothermal calcite is expected to provide radiocarbon-dead DIC decreasing the normalized ^{14}C content of riverine DIC relative to expectations from DIC derived from the atmosphere and/or soil respiration. Unlike $\delta^{13}C$, ^{14}C measurements expressed as pMC are unaffected by mass-dependent fractionation during degassing (McNichol & Aluwihare, 2007) and are thus easier to interpret as a constraint on DIC sources.

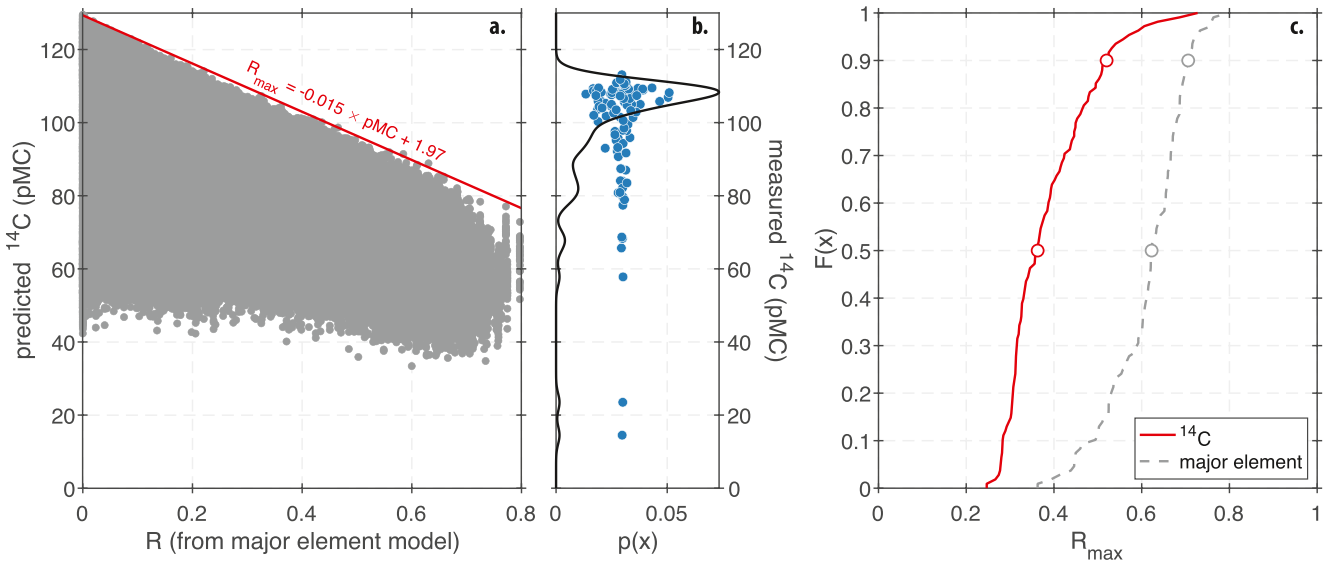

Figure 10. Carbon isotopic modeling. (a) The gray points show predictions of ^{14}C based on MEANDIR output for all 108 samples with C isotopic measurements. The red line shows a fitted upper bound based on all samples and simulations. (b) Field measurements of the ^{14}C content of dissolved inorganic carbon for the subset of river measurements presented by Sveinbjörnsdóttir et al. (2020) that also have major element data. The blue points show the individual measurements while the black line shows a kernel density estimate of their probability distribution. (c) Empirical cumulative distribution functions of the maximum allowable value of R_{net} based on modeling major elements using MEANDIR (gray dashed line) or a combination of MEANDIR and ^{14}C data (red line).

As a proof-of-concept, we use our model output from MEANDIR to predict the normalized ^{14}C content of DIC taking into account uncertainties in the isotopic composition of soil respiration using soil carbon data from Torres et al. (2020). We then compare these predictions to riverine measurements of normalized ^{14}C from Sveinbjörnsdóttir et al. (2020), which are available for 108 of the samples in our database with measurements of major element concentrations and MEANDIR model predictions. A full description of this calculation is included in Supporting Information S1. Unfortunately, there is no overlap between samples with measurements of Mg, Si, Ca, and Sr isotopic ratios and those with ^{14}C measurements, but we suggest that this would be a useful goal for future work.

For the 108 samples with ^{14}C measurements, we find that there is a shared upper bound where the highest normalized ^{14}C value that can be generated depends on R_{net} (Figure 10a). By fitting this upper bound with a linear relationship (Figure 10a), we are able to convert all of the measurements of ^{14}C (Figure 10b) into estimates of the maximum allowable R_{net} for each sample. We find that measurements of ^{14}C greatly decrease the highest allowable value of R_{net} based on major element constraints for most samples (Figure 10c). For example, 90% of samples with C isotopic data have maximum R_{net} values of less that 0.52 with most having maximum R_{net} less than 0.4 (Figure 10c).

River samples in the Sveinbjörnsdóttir et al. (2020) data set are super-saturated with respect to CO_2, have similar degrees of CO_2 super-saturation to soil pore waters, and can have δ^{13}C values that do not match equilibrium with atmospheric CO_2. Icelandic rivers also tend to have low concentrations of dissolved organic carbon (Bjarnadottir et al., 2021; Kardjilov et al., 2006) that could serve as an additional source of ^{14}C-enriched C decoupled from weathering processes. Consequently, the high normalized ^{14}C values are unlikely to represent exchange with atmospheric CO_2 or in situ respiration and instead can be reasonably be interpreted as a constraint on weathering processes. Assuming that the isotopic composition of riverine DIC in Iceland primarily reflects weathering processes, the high measured values of ^{14}C for most samples are incompatible with large carbonate contributions to the alkalinity budget (Figure 10c).

To further constrain R_{net}, we take advantage of the fact that some of the samples in our data set are time-series collected from single locations. Temporal variability in river chemistry has been attributed to the mixing of different water sources with relatively constant compositions (Stewart et al., 2022). Here, we extend this logic and posit that the different water sources in a catchment will share some of the same end-member solute sources. This hypothesis can be applied to a time-series to constrain R_{net} by removing simulations from each individual sample

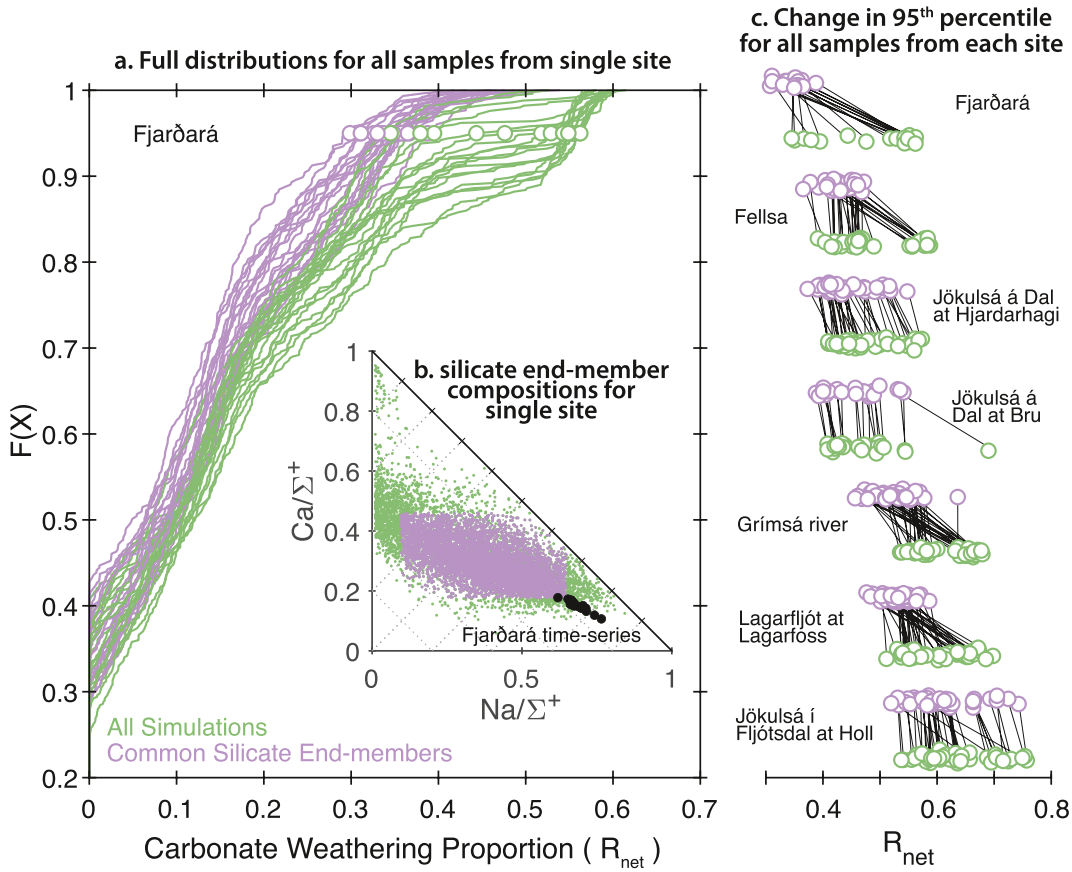

Figure 11. Constraining the carbonate weathering proportion (R_{net}) using time-series data. (a) Empirical cumulative distributions of R_{net} for all time-series samples from a single site along the Fjarðará River (Eiriksdottir et al., 2013). The green curves show all model simulations while the purple curves show the subset of model simulations with the same range of silicate end-member compositions. (b) Silicate end-member compositions from the Fjarðará showing the full range (green) and the range shared by all samples from the time-series (purple). (c) Change in the 95th percentile of R_{net} for all sites with long time-series after requiring all samples from a site to share the same range in silicate end-member compositions.

where the calculated silicate end-member composition is not shared with every other sample from the same location. This approach may be reasonable for sites like Iceland where bedrock is present at or near the surface and soils are relatively thin and poorly developed. We select the seven sites with at least 20 time-series measurements and investigate how the distribution of R_{net} changes when the constraint of shared silicate end-member compositions is imposed for each site.

For each of the seven sites, we find that the 95th percentile of the distribution of R_{net} values tends to decrease when all samples are required to sample the same silicate end-members (Figures 11a and 11c). The magnitude of the decrease is variable sample to sample and, in some instances, little to no change is observed. At the same time, we do not observe any samples where the 95th percentile is meaningfully increased (Figure 11c). While imposing shared silicate end-members on each time-series is an assumption, we note that mixing trends apparent in the data set are not inconsistent with shared end-members (Figure 11b). Given that high values of R_{net} are rare overall and that including additional constraints has a tendency to further decrease R_{net}, we conclude most of the alkalinity generated by chemical weathering in Iceland is sourced from the dissolution of silicates as opposed to carbonates.

4.3.1. Net Versus Gross Carbonate Contributions

The evidence for cation uptake into secondary phases during chemical weathering in Iceland implies that the partitioning of solutes between carbonate and silicate sources can be done for both gross (before secondary phase formation) and net (after secondary phase formation) weathering fluxes (Kemeny & Torres, 2021). These two approaches to source partitioning need not yield identical results given that (a) carbonate and silicate minerals

contribute differently to the budget of each major cation and (b) secondary phases preferentially uptake specific cations. Since Icelandic carbonates are observed to have low K and Mg contents (Harstad & Stipp, 2007) and secondary phases in Icelandic soil/sediment are K- and Mg-rich (Moulton et al., 2000; Thorpe et al., 2019), net weathering fluxes should show a higher contribution from carbonates relative to gross fluxes.

As expected, we find that secondary phase formation increases the net proportion of carbonate weathering (Figure 9c). The exact increase in R_{net} is uncertain and variable between samples, but increases of up to 20% are typically allowable (Figure 9c). So, estimates of carbonate contributions in Iceland may be elevated *because* of secondary phase formation and not just the abundance and reactivity of carbonate in the weathering zone. We also note that some samples show model solutions with ratios of net to gross carbonate proportions that are lower than one, which reflects the incorporation of carbonate derived Ca into secondary phases, which is discussed further below.

4.4. Implications of Incongruent Weathering for Cation Mobility

In prior publications on data from Icelandic rivers (e.g., Gíslason et al., 1996; Stefánsson & Gíslason, 2001), the "mobility" of different elements during weathering has been calculated as:

$$X\text{mobility} = 100 \times \frac{X^*/Na^*_{\text{river}}}{X/Na_{\text{basalt}}} \tag{7}$$

where the superscript asterisk refers to solute concentrations that have been corrected for contributions from atmospheric deposition using Cl concentrations and end-member element to Cl ratios. This approach conflates both types of incongruent weathering by assuming that the expected ratio of solutes in river waters (after correction for atmospheric contributions) is given by bulk basalts. As described above, our data suggests that the effective silicate end-member for most rivers in Iceland is not bulk basalts and is instead more Na-rich. As a result, the elemental mobility inferred from Equation 7 might be distinct from what is calculated using our approach. Identifying potential differences is important as they underlie the calibration of some isotopic tools for reconstructing weathering processes in the past (e.g., δ^7Li; Pogge von Strandmann, Fraser, et al., 2019).

Past estimates of element mobility in Iceland using Equation 7 are difficult to directly compare to our results using the solute mass balance model for multiple reasons. First, Equation 7 produces mobility values greater than 100% for some elements in some river samples (Stefánsson & Gíslason, 2001). Additionally, our solute mass balance model allows solutes sourced from rainwater or carbonates to ultimately be incorporated into clays, which is not accounted for in Equation 7. Such behavior is consistent with measurements of soil profiles in other volcanic landscapes where atmosphere-derived cations are incorporated into solid-phases (Chadwick et al., 2009; Dessert et al., 2020; Huh et al., 2004). The large uncertainty in our estimates of mobility for individual samples also makes it difficult to quantify biases that might result from Equation 7. For example, uncertainty in clay compositions and other model parameters can increase mobility estimates relative to what is predicted using Equation 7 despite the fact that a more Na-rich silicate end-member tends to decrease mobility estimates in general.

To make a simplified comparison to previous work, we note that Gíslason et al. (1996) report that K is more mobile than Ca in Icelandic watersheds, which is not supported by our analysis (Figures 7c and 7d). Similarly, Gíslason et al. (1996) suggest that up to 90% of Ca is sequestered into clays, which is a much higher proportion than our upper bound of less than 70% (Figure 7d). Superficially, our results appear more similar to what is reported in Stefánsson and Gíslason (2001) for overall mobility ranges, though we still expect to find differences between our different approaches on the level of individual samples. Additional constraints on clay compositions in Iceland as well as the degree and character of primary incongruence will likely be useful to better constrain solute mobility in Icelandic watersheds.

4.5. Processes Affecting Glacial Versus Non-Glacial Rivers

The results of the solute mass balance model are uncertain, but the few samples with the highest median carbonate contributions are from glacierized catchments (Figures 12a and 12b). Though this is apparently consistent with the hypothesis of Jacobson et al. (2015) that contributions from trace reactive phases are enhanced by glaciers in Iceland, we note that the majority of glacial rivers in our database do *not* show evidence for elevated carbonate

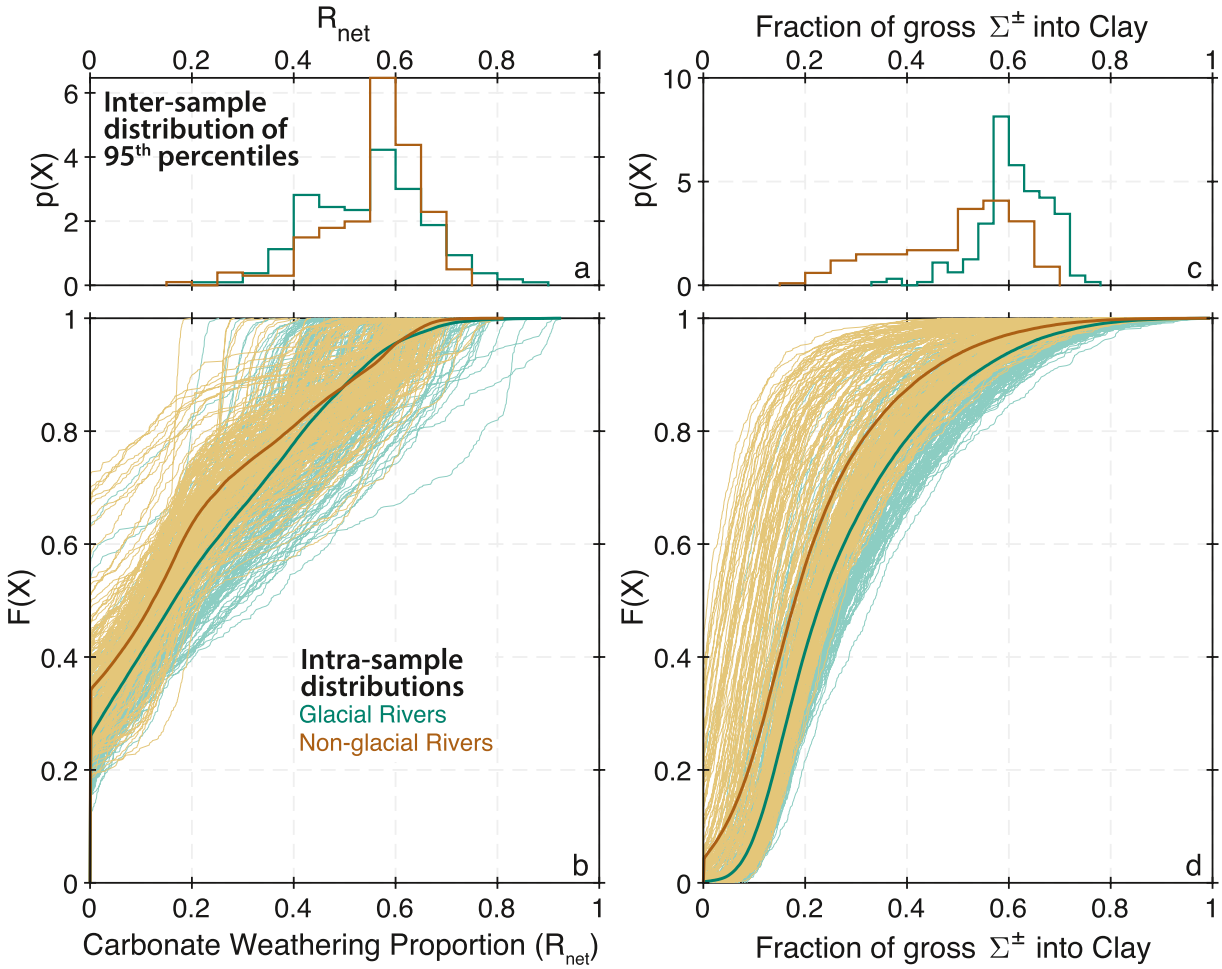

Figure 12. Solute mass balance model predictions for glaciated versus non-glaciated watersheds. (a) Inter-sample distribution of 95th percentile values for the proportion of carbonate weathering (R_{net}) for glaciated (blue) and non-glaciated (brown) river samples. (b) Full distributions of R_{net} for all glacial and non-glacial river samples. The thin, lighter-colored lines show individual samples whereas the thicker, darker-colored lines show the distributions for all samples combined. Panel (c) same as in panel (a), but showing the inter-sample distributions for the fraction of $\Sigma^+ + SO_4$ uptake into clays $\left(F_{clay}^{\Sigma\pm}\right)$. Panel (d) same as in panel (b) but showing the full distributions of $F_{clay}^{\Sigma\pm}$ for glaciated and non-glaciated watersheds.

contributions relative to non-glacial rivers (Figure 12b). Specifically, the inter-sample distributions of 95th percentile values for glacial versus non-glacial rivers are not substantially different from each other (Figure 12a).

The results of our solute mass balance model do not rule out the hypothesis of Hindshaw et al. (2013) that glaciation enhances secondary phase formation as the proportion of the total cation budget taken up into secondary phases may be slightly elevated in the glacierized catchments relative to non-glacial rivers (Figures 12c and 12d). Specifically, despite substantial overlap, the inter-sample distribution of 95th percentile values for $F_{clay}^{\pm}$ is shifted to higher values for the the glacial river samples compared to those from non-glaciated watersheds (Figure 12c).

Not all basalts contain significant carbonate as its formation is restricted to the portions of geothermal systems that experience boiling (Arnórsson, 1989; Neuhoff et al., 1999; Weisenberger & Selbekk, 2009). So, the observation that most of river water samples from Iceland, including those from glaciated watersheds, do not show evidence for large carbonate contributions could imply a heterogeneous distribution of different hydrothermal alteration minerals rather than an effect of distinctive surface processes on chemical weathering (i.e., glacial vs. fluvial erosion). The idea that glaciation enhances cation uptake into secondary phases (Hindshaw et al., 2013) is not expected and, technically, not required by the results of our analysis. However, it is consistent with the results of our solute mass balance model and the higher degree of secondary clay mineral super-saturation observed for river water samples from glaciated catchments (Figure S7 in Supporting Information S1).

4.6. Implications for the Long-Term C Cycle

The general Na enrichment of the river waters on account of both types of incongruent weathering may have implications for the long-term C cycle. At timescales shorter than or similar to the residence time of Ca, all silicate-derived alkalinity will impact atmospheric pCO_2 through its effects on the oceanic carbonate system (Middelburg et al., 2020). The unclear fate of silicate-derived Na and uncertainty in the timescale(s) associated with its removal processes (e.g., "reverse" weathering; Mackenzie, 1995) complicate longer-term inferences about its role in the global C cycle. Nevertheless, assuming that reverse weathering processes are "slow" relative to carbonate burial, which is not altogether unreasonable on account of the longer oceanic residence time of Na relative to Ca, the transient effect of increased silicate Na fluxes on atmospheric CO_2 may be long relative to climate and carbon cycle perturbations observed in geologic history. In general, the abundance of silicate-derived Na in weathering "hot spots" such as Iceland highlights the need for future research on how to best account for all silicate-derived alkalinity in the global C cycle.

5. Conclusions

While the chemistry of Icelandic waters has been extensively studied in the past, no previous analyses have used an inverse model that simultaneously allows for a solute sink, variable silicate end-member compositions, and key additional solute sources like carbonates and hydrothermal fluids. Such models are necessary as neglecting to include all processes can significantly bias model results (Bickle et al., 2015; Emberson et al., 2017, 2018). Using this approach, we find evidence that the silicate mineral dissolution in Iceland does not release solutes in the same proportions as bulk basalts and that this primary mineral incongruent weathering is further enhanced by the formation of cation-bearing secondary phases. These findings imply that some previous estimates of cation mobility in Iceland may have over-estimated the role of clays as solute sinks.

Our results also constrain the potential magnitude of carbonate contributions in Icelandic watersheds and suggest that silicate contributions dominate overall such that Iceland is an important locus of CO_2 draw down. In part, this may reflect the heterogeneous distribution of hydrothermal calcite given its specific formation mechanisms and the observation that only a few samples within our database are consistent with large carbonate contributions.

The bedrock lithology of Iceland is comparatively simple to other rivers with mixed igneous and sedimentary bedrock. The complexity of weathering processes identified using our analysis thus highlights the need for using more robust inverse approaches when attempting to partition solutes between carbonate and silicate sources. To improve upon our results, we recommend incorporating constraints from co-located measurements of solid-phase compositions and isotopic ratios into the inverse analysis of water chemistry data.

Data Availability Statement

The basalt and rhyolite bulk geochemistry data used in this study is available at http://georoc.mpch-mainz.gwdg.de/georoc/. The fine-grained sediment data used in this study is available in the original publications (Moulton et al., 2000; Thorpe et al., 2019). The hydrochemistry data used in this study are archived on GitHub (github.com/torres-lab/Cole_Iceland_JGR) along with the analysis code (Torres, 2022). The MEANDIR model code (version 1.2) is available at github.com/PrestonCosslettKemeny/MEANDIR. The MEANDIR input files (Torres, 2022) used in this study are archived on GitHub (github.com/torres-lab/Cole_Iceland_JGR).

Acknowledgments
Torres acknowledges support from the Sloan Foundation and NSF-EAR 2017106. Cole acknowledges support from the Mills Bennett Fellowship. Kemeny acknowledges support from the Fannie and John Hertz Foundation Cohan-Jacobs and Stein Families Fellowship and the National Defense Science and Engineering Graduate (NDSEG) Fellowship (DoD, Air Force Office of Scientific Research, 32 CFR 168a). All authors thank Drs. Cin-Ty Lee, Kirsten Siebach, and Laurence Yeung for helpful comments prior to submission.

References

Andrews, M. G., & Jacobson, A. D. (2017). The radiogenic and stable Sr isotope geochemistry of basalt weathering in Iceland: Role of hydrothermal calcite and implications for long-term climate regulation. *Geochimica et Cosmochimica Acta*, *215*, 247–262. https://doi.org/10.1016/j.gca.2017.08.012

Arnórsson, S. (1989). Deposition of calcium carbonate minerals from geothermal waters—Theoretical considerations. *Geothermics*, *18*(1–2), 33–39. https://doi.org/10.1016/0375-6505(89)90007-2

Arnórsson, S., Gunnarsson, I., Stefánsson, A., Andrésdóttir, A., & Sveinbjörnsdóttir, A. E. (2002). Major element chemistry of surface- and ground waters in basaltic terrain, N-Iceland. I. Primary mineral saturation. *Geochimica et Cosmochimica Acta*, *66*(23), 4015–4046. https://doi.org/10.1016/s0016-7037(02)00991-2

Baronas, J. J., West, A. J., Burton, K. W., Hammond, D. E., Opfergelt, S., Pogge von Strandmann, P. A., et al. (2020). Ge and Si isotope behavior during intense tropical weathering and ecosystem cycling. *Global Biogeochemical Cycles*, *34*(8), e2019GB006522. https://doi.org/10.1029/2019gb006522

Berner, R. A., Lasaga, A. C., & Garrels, R. M. (1983). The carbonate-silicate geochemical cycle and its effect on atmospheric carbon dioxide over the past 100 million years. *American Journal of Science*, *283*(7), 641–683. https://doi.org/10.2475/ajs.283.7.641

Bickle, M. J., Tipper, E. D., Galy, A., Chapman, H., & Harris, N. (2015). On discrimination between carbonate and silicate inputs to Himalayan rivers. *American Journal of Science*, *315*(2), 120–166. https://doi.org/10.2475/02.2015.02

Bjarnadottir, B., Sungur, G. A., Sigurdsson, B. D., Kjartansson, B. T., Oskarsson, H., Oddsdottir, E. S., et al. (2021). Carbon and water balance of an afforested shallow drained peatland in Iceland. *Forest Ecology and Management*, *482*, 118861. https://doi.org/10.1016/j.foreco.2020.118861

Blattmann, T. M., Wang, S.-L., Lupker, M., Märki, L., Haghipour, N., Wacker, L., et al. (2019). Sulphuric acid-mediated weathering on Taiwan buffers geological atmospheric carbon sinks. *Scientific Reports*, *9*(1), 1–8. https://doi.org/10.1038/s41598-019-39272-5

Bluth, G. J. S., & Kump, L. R. (1994). Lithologic and climatologic controls of river chemistry. *Geochimica et Cosmochimica Acta*, *58*(10), 2341–2359. https://doi.org/10.1016/0016-7037(94)90015-9

Börker, J., Hartmann, J., Romero-Mujalli, G., & Li, G. (2019). Aging of basalt volcanic systems and decreasing CO_2 consumption by weathering. *Earth Surface Dynamics*, *7*(1), 191–197. https://doi.org/10.5194/esurf-7-191-2019

Bouchez, J., von Blanckenburg, F., & Schuessler, J. A. (2013). Modeling novel stable isotope ratios in the weathering zone. *American Journal of Science*, *313*(4), 267–308. https://doi.org/10.2475/04.2013.01

Brantley, S. L., Kubicki, J. D., & White, A. F. (2008). In S. L. Brantley, J. D. Kubicki, & A. F. White (Eds.), *Kinetics of water-rock interaction*. Springer.

Brazier, J.-M., Schmitt, A.-D., Gangloff, S., Pelt, E., Chabaux, F., & Tertre, E. (2019). Calcium isotopic fractionation during adsorption onto and desorption from soil phyllosilicates (kaolinite, montmorillonite and muscovite). *Geochimica et Cosmochimica Acta*, *250*, 324–347. https://doi.org/10.1016/j.gca.2019.02.017

Broecker, W. S., & Sanyal, A. (1998). Does atmospheric CO_2 police the rate of chemical weathering? *Global Biogeochemical Cycles*, *12*(3), 403–408. https://doi.org/10.1029/98gb01927

Chadwick, O., Derry, L., Bern, C., & Vitousek, P. (2009). Changing sources of strontium to soils and ecosystems across the Hawaiian Islands. *Chemical Geology*, *267*(1–2), 64–76. https://doi.org/10.1016/j.chemgeo.2009.01.009

Chen, Y., & Brantley, S. L. (1997). Temperature-and pH-dependence of albite dissolution rate at acid pH. *Chemical Geology*, *135*(3–4), 275–290. https://doi.org/10.1016/s0009-2541(96)00126-x

Condomines, M., Grönvold, K., Hooker, P., Muehlenbachs, K., O'Nions, R., Oskarsson, N., & Oxburgh, E. (1983). Helium, oxygen, strontium and neodymium isotopic relationships in Icelandic volcanics. *Earth and Planetary Science Letters*, *66*, 125–136. https://doi.org/10.1016/0012-821x(83)90131-0

Cornelis, J.-T., Weis, D., Lavkulich, L., Vermeire, M.-L., Delvaux, B., & Barling, J. (2014). Silicon isotopes record dissolution and re-precipitation of pedogenic clay minerals in a podzolic soil chronosequence. *Geoderma*, *235–236*, 19–29. https://doi.org/10.1016/j.geoderma.2014.06.023

Crovisier, J.-L., Honnorez, J., Fritz, B., & Petit, J.-C. (1992). Dissolution of subglacial volcanic glasses from Iceland: Laboratory study and modelling. *Applied Geochemistry*, *7*, 55–81. https://doi.org/10.1016/s0883-2927(09)80064-4

Dellinger, M., Gaillardet, J., Bouchez, J., Calmels, D., Louvat, P., Dosseto, A., et al. (2015). Riverine Li isotope fractionation in the Amazon River basin controlled by the weathering regimes. *Geochimica et Cosmochimica Acta*, *164*, 71–93. https://doi.org/10.1016/j.gca.2015.04.042

Dessert, C., Clergue, C., Rousteau, A., Crispi, O., & Benedetti, M. F. (2020). Atmospheric contribution to cations cycling in highly weathered catchment, Guadeloupe (Lesser Antilles). *Chemical Geology*, *531*, 119354. https://doi.org/10.1016/j.chemgeo.2019.119354

Dessert, C., Dupre, B., Gaillardet, J., Francois, L. M. M., & Allegre, C. J. J. (2003). Basalt weathering laws and the impact of basalt weathering on the global carbon cycle. *Chemical Geology*, *202*(3–4), 257–273. https://doi.org/10.1016/j.chemgeo.2002.10.001

Druhan, J. L., & Maher, K. (2017). The influence of mixing on stable isotope ratios in porous media: A revised Rayleigh model. *Water Resources Research*, *53*(2), 1101–1124. https://doi.org/10.1002/2016wr019666

Ehlmann, B., Bish, D., Ruff, S., & Mustard, J. (2012). Mineralogy and chemistry of altered Icelandic basalts: Application to clay mineral detection and understanding aqueous environments on Mars. *Journal of Geophysical Research*, *117*(E11), E00J16. https://doi.org/10.1029/2012je004156

Eiriksdottir, E. S., Gislason, S. R., & Oelkers, E. H. (2013). Does temperature or runoff control the feedback between chemical denudation and climate? Insights from NE Iceland. *Geochimica et Cosmochimica Acta*, *107*, 65–81. https://doi.org/10.1016/j.gca.2012.12.034

Elderfield, H., & Greaves, M. J. (1981). Strontium isotope geochemistry of Icelandic geothermal systems and implications for sea water chemistry. *Geochimica et Cosmochimica Acta*, *45*(11), 2201–2212. https://doi.org/10.1016/0016-7037(81)90072-7

Emberson, R., Galy, A., & Hovius, N. (2017). Combined effect of carbonate and biotite dissolution in landslides biases silicate weathering proxies. *Geochimica et Cosmochimica Acta*, *213*, 418–434. https://doi.org/10.1016/j.gca.2017.07.014

Emberson, R., Galy, A., & Hovius, N. (2018). Weathering of reactive mineral phases in landslides acts as a source of carbon dioxide in mountain belts. *Journal of Geophysical Research: Earth Surface*, *123*(10), 2695–2713. https://doi.org/10.1029/2018jf004672

Ferrier, K. L., & Kirchner, J. W. (2008). Effects of physical erosion on chemical denudation rates: A numerical modeling study of soil-mantled hillslopes. *Earth and Planetary Science Letters*, *272*(3–4), 591–599. https://doi.org/10.1016/j.epsl.2008.05.024

Gaillardet, J., Dupré, B., Louvat, P., & Allegre, C. J. (1999). Global silicate weathering and CO_2 consumption rates deduced from the chemistry of large rivers. *Chemical Geology*, *159*(1–4), 3–30. https://doi.org/10.1016/s0009-2541(99)00031-5

Gannoun, A., Burton, K. W., Vigier, N., Gíslason, S. R., Rogers, N., Mokadem, F., & Sigfússon, B. (2006). The influence of weathering process on riverine osmium isotopes in a basaltic terrain. *Earth and Planetary Science Letters*, *243*(3–4), 732–748. https://doi.org/10.1016/j.epsl.2006.01.024

Garrels, R. M., & Mackenzie, F. T. (1967). Origin of the chemical compositions of some springs and lakes. *Equilibrium concepts in natural water systems* (pp. 222–242).

Geilert, S., Vroon, P. Z., Keller, N. S., Gudbrandsson, S., Stefánsson, A., & van Bergen, M. J. (2015). Silicon isotope fractionation during silica precipitation from hot-spring waters: Evidence from the Geysir geothermal field, Iceland. *Geochimica et Cosmochimica Acta*, *164*, 403–427. https://doi.org/10.1016/j.gca.2015.05.043

Georg, R. B., Reynolds, B. C., West, A. J., Burton, K. W., & Halliday, A. N. (2007). Silicon isotope variations accompanying basalt weathering in Iceland. *Earth and Planetary Science Letters*, *261*(3–4), 476–490. https://doi.org/10.1016/j.epsl.2007.07.004

Gíslason, S. R., Arnórsson, S., & Ármannsson, H. (1996). Chemical weathering of basalt in southwest Iceland: Effects of runoff, age of rocks and vegetative/glacial cover. *American Journal of Science*, *296*(8), 837–907. https://doi.org/10.2475/ajs.296.8.837

Gislason, S. R., & Arnórsson, S. (1993). Dissolution of primary basaltic minerals in natural waters: Saturation state and kinetics. *Chemical Geology*, *105*(1–3), 117–135. https://doi.org/10.1016/0009-2541(93)90122-y

Gislason, S. R., & Eugster, H. P. (1987). Meteoric water-basalt interactions. I: A laboratory study. *Geochimica et Cosmochimica Acta*, *51*(10), 2827–2840. https://doi.org/10.1016/0016-7037(87)90161-x

Gislason, S. R., & Oelkers, E. H. (2003). Mechanism, rates, and consequences of basaltic glass dissolution: II. An experimental study of the dissolution rates of basaltic glass as a function of pH and temperature. *Geochimica et Cosmochimica Acta*, *67*(20), 3817–3832. https://doi.org/10.1016/S0016-7037(03)00176-5

Gíslason, S. R., Snorrason, A., Ingvarsson, G. B., Sigfússon, B., Eiríksdóttir, E. S., Elefsen, S., et al. (2006). *Chemical composition, discharge and suspended matter of rivers in North-Western Iceland: The database of the Science Institute, University of Iceland, and the Hydrological Service of the National Energy Authority*. Raunvísindastofnun Háskólans.

Gislason, S. R., & Torssander, P. (2006). Response of sulfate concentration and isotope composition in Icelandic rivers to the decline in global atmospheric SO_2 emissions into the North Atlantic region. *Environmental Science and Technology*, *40*(3), 680–686. https://doi.org/10.1021/es051325o

Gudbrandsson, S., Wolff-Boenisch, D., Gíslason, S. R., & Oelkers, E. H. (2008). Dissolution rates of crystalline basalt at pH 4 and 10 and 25–75°C. *Mineralogical Magazine*, *72*(1), 155–158. https://doi.org/10.1180/minmag.2008.072.1.155

Harstad, A., & Stipp, S. L. S. (2007). Calcite dissolution: Effects of trace cations naturally present in Iceland spar calcites. *Geochimica et Cosmochimica Acta*, *71*(1), 56–70. https://doi.org/10.1016/j.gca.2006.07.037

Hemingway, J. D., Olson, H., Turchyn, A. V., Tipper, E. T., Bickle, M. J., & Johnston, D. T. (2020). Triple oxygen isotope insight into terrestrial pyrite oxidation. *Proceedings of the National Academy of Sciences*, *117*(14), 7650–7657. https://doi.org/10.1073/pnas.1917518117

Hemond, C., Condomines, M., Fourcade, S., Allègre, C., Oskarsson, N., & Javoy, M. (1988). Thorium, strontium and oxygen isotopic geochemistry in recent tholeiites from Iceland: Crustal influence on mantle-derived magmas. *Earth and Planetary Science Letters*, *87*(3), 273–285. https://doi.org/10.1016/0012-821x(88)90015-5

Hindshaw, R. S., Bourdon, B., Pogge von Strandmann, P. A., Vigier, N., & Burton, K. W. (2013). The stable calcium isotopic composition of rivers draining basaltic catchments in Iceland. *Earth and Planetary Science Letters*, *374*, 173–184. https://doi.org/10.1016/j.epsl.2013.05.038

Hindshaw, R. S., Tosca, R., Tosca, N. J., & Tipper, E. T. (2020). Experimental constraints on mg isotope fractionation during clay formation: Implications for the global biogeochemical cycle of Mg. *Earth and Planetary Science Letters*, *531*, 115980. https://doi.org/10.1016/j.epsl.2019.115980

Huh, Y., Chan, L.-H., & Chadwick, O. A. (2004). Behavior of lithium and its isotopes during weathering of Hawaiian basalt. *Geochemistry, Geophysics, Geosystems*, *5*(9), Q09002. https://doi.org/10.1029/2004gc000729

Ibarra, D. E., Caves, J. K., Moon, S., Thomas, D. L., Hartmann, J., Chamberlain, C. P., & Maher, K. (2016). Differential weathering of basaltic and granitic catchments from concentration–discharge relationships. *Geochimica et Cosmochimica Acta*, *190*, 265–293. https://doi.org/10.1016/j.gca.2016.07.006

Jacobson, A. D., Grace Andrews, M., Lehn, G. O., & Holmden, C. (2015). Silicate versus carbonate weathering in Iceland: New insights from Ca isotopes. *Earth and Planetary Science Letters*, *1*, 1–11. https://doi.org/10.1016/j.epsl.2015.01.030

Kardjilov, M., Gisladottir, G., & Gislason, S. (2006). Land degradation in northeastern Iceland: Present and past carbon fluxes. *Land Degradation & Development*, *17*(4), 401–417. https://doi.org/10.1002/ldr.746

Kemeny, P. C., Lopez, G., Dalleska, N., Torres, M., Burke, A., Bhatt, M., et al. (2020). Sulfate sulfur isotopes and major ion chemistry reveal that pyrite oxidation counteracts CO_2 drawdown from silicate weathering in the Langtang-Trisuli-Narayani River system, Nepal Himalaya. *Geochimica et Cosmochimica Acta*, *294*, 43–69. https://doi.org/10.1016/j.gca.2020.11.009

Kemeny, P. C., & Torres, M. (2021). Presentation and applications of modeling elements and dissolved isotopes in rivers (MEANDIR), a customizable MATLAB model for Monte Carlo inversion of dissolved river chemistry. *American Journal of Science*, *321*(5), 579–642. https://doi.org/10.2475/05.2021.03

Kemeny, P. C., Torres, M. A., Lamb, M. P., Webb, S. M., Dalleska, N., Cole, T., et al. (2021). Organic sulfur fluxes and geomorphic control of sulfur isotope ratios in rivers. *Earth and Planetary Science Letters*, *562*, 116838. https://doi.org/10.1016/j.epsl.2021.116838

Larsen, G., & Eiriksson, J. (2008). Late Quaternary terrestrial tephrochronology of Iceland—Frequency of explosive eruptions, type and volume of tephra deposits. *Journal of Quaternary Science: Published for the Quaternary Research Association*, *23*(2), 109–120. https://doi.org/10.1002/jqs.1129

Li, D., Jacobson, A. D., & McInerney, D. J. (2014). A reactive-transport model for examining tectonic and climatic controls on chemical weathering and atmospheric CO_2 consumption in granitic regolith. *Chemical Geology*, *365*, 30–42. https://doi.org/10.1016/j.chemgeo.2013.11.028

Li, G., & Elderfield, H. (2013). Evolution of carbon cycle over the past 100 million years. *Geochimica et Cosmochimica Acta*, *103*, 11–25. https://doi.org/10.1016/j.gca.2012.10.014

Li, G., Hartmann, J., Derry, L. A., West, A. J., You, C.-F., Long, X., et al. (2016). Temperature dependence of basalt weathering. *Earth and Planetary Science Letters*, *443*, 59–69. https://doi.org/10.1016/j.epsl.2016.03.015

Louvat, P., Gislason, S. R., & Allègre, C. J. (2008). Chemical and mechanical erosion rates in Iceland as deduced from river dissolved and solid material. *American Journal of Science*, *308*(5), 679–726. https://doi.org/10.2475/05.2008.02

Mackenzie, F. T., & Garrels, R. (1966). Chemical mass balance between rivers and oceans. *American Journal of Science*, *264*(7), 19–525. https://doi.org/10.2475/ajs.264.7.507

Mackenzie, F. T., & Kump, L. R. (1995). Reverse weathering, clay mineral formation, and oceanic element cycles. *Science*, *270*(5236), 586–587. https://doi.org/10.1126/science.270.5236.586

McNichol, A. P., & Aluwihare, L. I. (2007). The power of radiocarbon in biogeochemical studies of the marine carbon cycle: Insights from studies of dissolved and particulate organic carbon (DOC and POC). *Chemical Reviews*, *107*(2), 443–466. https://doi.org/10.1002/chin.200724246

Meyer, P. S., & Sigurdsson, H. (1978). Interstitial acid glass and chlorophaeite in Iceland basalts. *Lithos*, *11*(3), 231–241. https://doi.org/10.1016/0024-4937(78)90023-3

Middelburg, J. J., Soetaert, K., & Hagens, M. (2020). Ocean alkalinity, buffering and biogeochemical processes. *Reviews of Geophysics*, *58*(3), e2019RG000681. https://doi.org/10.1029/2019rg000681

Misra, S., & Froelich, P. N. (2012). Lithium isotope history of Cenozoic seawater: Changes in silicate weathering and reverse weathering. *Science*, *335*(6070), 818–823. https://doi.org/10.1126/science.1214697

Moon, S., Chamberlain, C. P., & Hilley, G. E. (2014). New estimates of silicate weathering rates and their uncertainties in global rivers. *Geochimica et Cosmochimica Acta*, *134*, 257–274. https://doi.org/10.1016/j.gca.2014.02.033

Moulton, K. L., West, J., & Berner, R. A. (2000). Solute flux and mineral mass balance approaches to the quantification of plant effects on silicate weathering. *American Journal of Science*, *300*(7), 539–570. https://doi.org/10.2475/ajs.300.7.539

Mutonga, M. W., Sveinbjornsdottir, A., Gislason, G., & Amannsson, H. (2010). The isotopic and chemical characteristics of geothermal fluids in Hengill Area, SW-Iceland (Hellisheidi, Hveragerdi and Nesjavellir Fields). In *Proceedings of the World Geothermal Congress, Bali, Indonesia* (pp. 1–13).

Négrel, P., Allegre, C. J., Dupré, B., & Lewin, E. (1993). Erosion sources determined by inversion of major and trace element ratios and strontium isotopic ratios in river water: The Congo Basin case. *Earth and Planetary Science Letters*, *120*(1–2), 59–76. https://doi.org/10.1016/0012-821x(93)90023-3

Neuhoff, P. S., Fridriksson, T., Arnorsson, S., & Bird, D. K. (1999). Porosity evolution and mineral paragenesis during low-grade metamorphism of basaltic lavas at Teigarhorn, eastern Iceland. *American Journal of Science*, *299*(6), 467–501. https://doi.org/10.2475/ajs.299.6.467

O'nions, R., & Grönvold, K. (1973). Petrogenetic relationships of acid and basic rocks in Iceland: Sr-isotopes and rare-earth elements in late and postglacial volcanics. *Earth and Planetary Science Letters*, *19*(4), 397–409. https://doi.org/10.1016/0012-821x(73)90182-9

Ockert, C., Gussone, N., Kaufhold, S., & Teichert, B. (2013). Isotope fractionation during Ca exchange on clay minerals in a marine environment. *Geochimica et Cosmochimica Acta*, *112*, 374–388. https://doi.org/10.1016/j.gca.2012.09.041

Olsson, J., Stipp, S., Makovicky, E., & Gislason, S. (2014). Metal scavenging by calcium carbonate at the Eyjafjallajökull volcano: A carbon capture and storage analogue. *Chemical Geology*, *384*, 135–148. https://doi.org/10.1016/j.chemgeo.2014.06.025

Opfergelt, S., Burton, K., Von Strandmann, P. P., Gislason, S., & Halliday, A. (2013). Riverine silicon isotope variations in glaciated basaltic terrains: Implications for the Si delivery to the ocean over glacial–interglacial intervals. *Earth and Planetary Science Letters*, *369*, 211–219. https://doi.org/10.1016/j.epsl.2013.03.025

Óskarsson, B. V., Riishuus, M. S., & Arnalds, Ó. (2012). Climate-dependent chemical weathering of volcanic soils in Iceland. *Geoderma*, *189*, 635–651. https://doi.org/10.1016/j.geoderma.2012.05.030

Óskarsson, F., Armannsson, H., Olafsson, M., Sveinbjornsdottir, A. E., & Markusson, S. H. (2013). The Theistareykir geothermal field, NE Iceland: Fluid chemistry and production properties. *Procedia Earth and Planetary Science*, *7*, 644–647. https://doi.org/10.1016/j.proeps.2013.03.185

Park, Y., Maffre, P., Goddéris, Y., Macdonald, F. A., Anttila, E. S., & Swanson-Hysell, N. L. (2020). Emergence of the Southeast Asian islands as a driver for Neogene cooling. *Proceedings of the National Academy of Sciences*, *117*(41), 25319–25326. https://doi.org/10.1073/pnas.2011033117

Pogge von Strandmann, P. A. E., Burton, K. W., James, R. H., van Calsteren, P., Gíslason, S. R., & Mokadem, F. (2006). Riverine behaviour of uranium and lithium isotopes in an actively glaciated basaltic terrain. *Earth and Planetary Science Letters*, *251*(1–2), 134–147. https://doi.org/10.1016/j.epsl.2006.09.001

Pogge von Strandmann, P. A. E., Burton, K. W., James, R. H., van Calsteren, P., Gislason, S. R., & Sigfusson, B. (2008). The influence of weathering processes on riverine magnesium isotopes in a basaltic terrain. *Earth and Planetary Science Letters*, *276*(1–2), 187–197. https://doi.org/10.1016/j.epsl.2008.09.020

Pogge von Strandmann, P. A. E., Fraser, W. T., Hammond, S. J., Tarbuck, G., Wood, I. G., Oelkers, E. H., & Murphy, M. J. (2019). Experimental determination of Li isotope behaviour during basalt weathering. *Chemical Geology*, *517*, 34–43. https://doi.org/10.1016/j.chemgeo.2019.04.020

Pogge von Strandmann, P. A. E., Olsson, J., Luu, T.-H., Gislason, S. u. R., & Burton, K. W. (2019). Using Mg isotopes to estimate natural calcite compositions and precipitation rates during the 2010 Eyjafjallajökull eruption. *Frontiers in Earth Science*, *7*, 6. https://doi.org/10.3389/feart.2019.00006

Rickli, J., Frank, M., Stichel, T., Georg, R. B., Vance, D., & Halliday, A. N. (2013). Controls on the incongruent release of hafnium during weathering of metamorphic and sedimentary catchments. *Geochimica et Cosmochimica Acta*, *101*, 263–284. https://doi.org/10.1016/j.gca.2012.10.019

Roerdink, D. L., van den Boorn, S. H., Geilert, S., Vroon, P. Z., & van Bergen, M. J. (2015). Experimental constraints on kinetic and equilibrium silicon isotope fractionation during the formation of non-biogenic chert deposits. *Chemical Geology*, *402*, 40–51. https://doi.org/10.1016/j.chemgeo.2015.02.038

Ruiz-Agudo, E., Putnis, C. V., Rodriguez-Navarro, C., & Putnis, A. (2012). Mechanism of leached layer formation during chemical weathering of silicate minerals. *Geology*, *40*(10), 947–950. https://doi.org/10.1130/g33339.1

Ryu, J. S., Jacobson, A. D., Holmden, C., Lundstrom, C., & Zhang, Z. (2011). The major ion, $\delta^{44}/^{40}$Ca, $\delta^{44}/^{42}$Ca, and $\delta^{26}/^{24}$Mg geochemistry of granite weathering at pH = 1 and T = 25°C: Power-law processes and the relative reactivity of minerals. *Geochimica et Cosmochimica Acta*, *75*(20), 6004–6026. https://doi.org/10.1016/j.gca.2011.07.025

Ryu, J.-S., Vigier, N., Lee, S.-W., Lee, K.-S., & Chadwick, O. A. (2014). Variation of lithium isotope geochemistry during basalt weathering and secondary mineral transformations in Hawaii. *Geochimica et Cosmochimica Acta*, *145*, 103–115. https://doi.org/10.1016/j.gca.2014.08.030

Savage, P. S., Georg, R. B., Williams, H. M., Burton, K. W., & Halliday, A. N. (2011). Silicon isotope fractionation during magmatic differentiation. *Geochimica et Cosmochimica Acta*, *75*(20), 6124–6139. https://doi.org/10.1016/j.gca.2011.07.043

Schaef, H., & McGrail, P. (2009). Dissolution of Columbia River Basalt under mildly acidic conditions as a function of temperature: Experimental results relevant to the geological sequestration of carbon dioxide. *Applied Geochemistry*, *24*(5), 980–987. https://doi.org/10.1016/j.apgeochem.2009.02.025

Scott, S., Gunnarsson, I., Arnórsson, S., & Stefánsson, A. (2014). Gas chemistry, boiling and phase segregation in a geothermal system, Hellisheidi, Iceland. *Geochimica et Cosmochimica Acta*, *124*, 170–189. https://doi.org/10.1016/j.gca.2013.09.027

Stefánsson, A., & Gíslason, S. R. (2001). Chemical weathering of basalts, southwest Iceland: Effect of rock crystallinity and secondary minerals on chemical fluxes to the ocean. *American Journal of Science*, *301*(6), 513–556. https://doi.org/10.2475/ajs.301.6.513

Stefánsson, A., Gíslason, S. R., & Arnórsson, S. (2001). Dissolution of primary minerals in natural waters II. Mineral saturation state. *Chemical Geology*, *172*(3–4), 251–276. https://doi.org/10.1016/s0009-2541(00)00262-x

Stewart, B., Shanley, J. B., Kirchner, J. W., Norris, D., Adler, T., Bristol, C., et al. (2022). Streams as mirrors: Reading subsurface water chemistry from stream chemistry. *Water Resources Research*, *58*(1), e2021WR029931. https://doi.org/10.1029/2021wr029931

Sun, S.-S., & Jahn, B.-M. (1975). Lead and strontium isotopes in post-glacial basalts from Iceland. *Nature*, *255*(5509), 527–530. https://doi.org/10.1038/255527a0

Sveinbjörnsdóttir, Á. E., Stefánsson, A., Heinemeier, J., Arnórsson, S., Eiríksdóttir, E. S., & Ólafsdóttir, R. (2020). Assessing the sources of inorganic carbon in surface-soil-and non-thermal groundwater in Iceland by δ^{13}C and ^{14}C. *Geochimica et Cosmochimica Acta*, *279*, 165–188. https://doi.org/10.1016/j.gca.2020.03.021

Taylor, A. S., Blum, J. D., & Lasaga, A. C. (2000). The dependence of labradorite dissolution and Sr isotope release rates on solution saturation state. *Geochimica et Cosmochimica Acta*, *64*(14), 2389–2400. https://doi.org/10.1016/s0016-7037(00)00361-6

Thorpe, M. T., Hurowitz, J. A., & Dehouck, E. (2019). Sediment geochemistry and mineralogy from a glacial terrain river system in southwest Iceland. *Geochimica et Cosmochimica Acta*, *263*, 140–166. https://doi.org/10.1016/j.gca.2019.08.003

Torres, M. A. (2022). Cole et al. data analysis code v1.0. [Software] (Technical Report). Zenodo. https://doi.org/10.5281/zenodo.3688815

Torres, M. A., Kemeny, P. C., Lamb, M. P., Cole, T. L., & Fischer, W. W. (2020). Long-term storage and age-biased export of fluvial organic carbon: Field evidence from west Iceland. *Geochemistry, Geophysics, Geosystems*, *21*(4), e2019GC008632. https://doi.org/10.1029/2019gc008632

Torres, M. A., West, A. J., Clark, K. E., Paris, G., Bouchez, J., Ponton, C., et al. (2016). The acid and alkalinity budgets of weathering in the Andes-Amazon system: Insights into the erosional control of global biogeochemical cycles. *Earth and Planetary Science Letters*, *450*, 381–391. https://doi.org/10.1016/j.epsl.2016.06.012

Vigier, N., Burton, K., Gislason, S., Rogers, N., Duchene, S., Thomas, L., et al. (2006). The relationship between riverine U-series disequilibria and erosion rates in a basaltic terrain. *Earth and Planetary Science Letters*, *249*(3–4), 258–273. https://doi.org/10.1016/j.epsl.2006.07.001

Vigier, N., Gislason, S., Burton, K., Millot, R., & Mokadem, F. (2009). The relationship between riverine lithium isotope composition and silicate weathering rates in Iceland. *Earth and Planetary Science Letters*, *287*(3–4), 434–441. https://doi.org/10.1016/j.epsl.2009.08.026

Wada, K., Arnalds, O., Kakuto, Y., Wilding, L., & Hallmark, C. (1992). Clay minerals of four soils formed in eolian and tephra materials in Iceland. *Geoderma*, *52*(3–4), 351–365. https://doi.org/10.1016/0016-7061(92)90046-a

Weisenberger, T., & Selbekk, R. S. (2009). Multi-stage zeolite facies mineralization in the Hvalfjördur area, Iceland. *International Journal of Earth Sciences*, *98*(5), 985–999. https://doi.org/10.1007/s00531-007-0296-6

West, A. J., Galy, A., & Bickle, M. (2005). Tectonic and climatic controls on silicate weathering. *Earth and Planetary Science Letters*, *235*(1–2), 211–228. https://doi.org/10.1016/j.epsl.2005.03.020

White, A. F., Bullen, T. D., Vivit, D. V., Schulz, M. S., & Clow, D. W. (1999). The role of disseminated calcite in the chemical weathering of granitoid rocks. *Geochimica et Cosmochimica Acta*, *63*(13), 1939–1953. https://doi.org/10.1016/s0016-7037(99)00082-4

White, A. F., Schulz, M. S., Lowenstern, J. B., Vivit, D. V., & Bullen, T. D. (2005). The ubiquitous nature of accessory calcite in granitoid rocks: Implications for weathering, solute evolution, and petrogenesis. *Geochimica et Cosmochimica Acta*, *69*(6), 1455–1471. https://doi.org/10.1016/j.gca.2004.09.012

Wilkinson, J., Reynolds, B., Neal, C., Hill, S., Neal, M., & Harrow, M. (1997). Major, minor and trace element composition of cloudwater and rainwater at Plynlimon. *Hydrology and Earth System Sciences*, *1*(3), 557–569. https://doi.org/10.5194/hess-1-557-1997

Wolff-Boenisch, D., Gislason, S. R., Oelkers, E. H., & Putnis, C. V. (2004). The dissolution rates of natural glasses as a function of their composition at pH 4 and 10.6, and temperatures from 25 to 745°C. *Geochimica et Cosmochimica Acta*, *68*(23), 4843–4858. https://doi.org/10.1016/j.gca.2004.05.027

Zheng, X.-Y., Beard, B. L., & Johnson, C. M. (2019). Constraining silicon isotope exchange kinetics and fractionation between aqueous and amorphous Si at room temperature. *Geochimica et Cosmochimica Acta*, *253*, 267–289. https://doi.org/10.1016/j.gca.2019.03.031

Ziegler, K., Chadwick, O. A., Brzezinski, M. A., & Kelly, E. F. (2005). Natural variations of δ^{30}Si ratios during progressive basalt weathering, Hawaiian Islands. *Geochimica et Cosmochimica Acta*, *69*(19), 4597–4610. https://doi.org/10.1016/j.gca.2005.05.008

Ziegler, K., Chadwick, O. A., White, A. F., & Brzezinski, M. A. (2005). δ^{30}Si systematics in a granitic saprolite, Puerto Rico. *Geology*, *33*(10), 817. https://doi.org/10.1130/g21707.1